The rice bundle sheath produces reactive oxygen species during high light stress via NADPH oxidase

Haiyan Xiong[1], Lei Hua[1], Ivan Reyna-Llorens[1], Yi Shi[2], Kun-Ming Chen[2], Nicholas Smirnoff[3], Johannes Kromdijk[1] and Julian M. Hibberd[1]

[1] Department of Plant Sciences, University of Cambridge, Downing Street, Cambridge CB2 3EA, United Kingdom.

[2] State Key Laboratory of Crop Stress Biology in Arid Area/College of Life Sciences, Northwest A&F University, Yangling, Shaanxi, 712100, China.

[3] College of Life and Environmental Sciences, University of Exeter, EX4 4QD, United Kingdom.

Email addresses:

HX - hx253@cam.ac.uk

LH - lh556@cam.ac.uk

I R-L – iar28@cam.ac.uk

YS - 17749124768@163.com

KC - kunmingchen@nwsuaf.edu.cn

NS - n.smirnoff@exeter.ac.uk

JK - jk417@cam.ac.uk

JMH - jmh65@cam.ac.uk

Running title: High light response of the rice bundle sheath

Keywords: rice; bundle sheath strands; reactive oxygen species; high light; mesophyll

Abstract

When exposed to high light plants produce reactive oxygen species (ROS). In *Arabidopsis thaliana* local accumulation of ROS preferentially takes place in bundle sheath strands, but little is known about how this response takes place. Using rice and the ROS probes diaminobenzidine and 2',7'-dichlorodihydrofluorescein diacetate, we found that after exposure to high light, ROS were produced more rapidly in bundle sheath strands than mesophyll cells. This response was not affected either by CO_2 supply or photorespiration. Consistent with these findings, deep sequencing of mRNA isolated from mesophyll or bundle sheath strands indicated balanced accumulation of transcripts encoding all major components of the photosynthetic apparatus. However, transcripts encoding several isoforms of the superoxide/H_2O_2-producing enzyme NADPH oxidase were more abundant in bundle sheath strands than mesophyll cells. ROS production in bundle sheath strands was reduced by blocking NADPH oxidase activity pharmacologically, but increased when the bundle sheath preferential *RBOHA* isoform of NADPH oxidase was over-expressed. NADPH oxidase mediated accumulation of ROS in the rice bundle sheath was detected in etiolated leaves lacking chlorophyll indicating that high light and NADPH oxidase-dependent ROS production is not dependent on photosynthesis.

Introduction

Under high-light conditions the capacity for light capture during photosynthesis can exceed use. This can lead to damage, generate signals promoting repair, and also initiate responses allowing acclimation (Asada, 1999; Li et al., 2009; Mullineaux et al., 2018). One source of damage is an increase in the production of reactive oxygen species (ROS). For example, oxygen photoreduction, largely at Photosystem I can result in superoxide and hydrogen peroxide. The other source is singlet oxygen which is formed by interaction of oxygen with triplet state chlorophyll in Photosystem II (Noctor and Foyer, 1998; Li et al., 2009; Murchie and Niyogi, 2011). As ROS are potentially harmful, with the ability to damage Fe-S proteins, oxidise amino acid residues and generate further radicals and reactive electrophiles resulting in lipid peroxidation and DNA damage, photosynthetic organisms have evolved a variety of mechanisms to minimize over-excitation of the photosystems. These range from transcriptional responses mediated by retrograde signaling between chloroplast and nucleus (Rossel et al., 2002; Kimura et al., 2003; Kleine et al., 2007; Li et al., 2009; Ruckle et al., 2012; Vogel et al., 2014; Dietz, 2015; Crisp et al., 2017; Mullineaux et al., 2018) to more immediate remodeling of light harvesting structures to dissipate excess excitation energy (Muller, 2001; Ruban, 2016).

Processes that dissipate energy in excess of that used by the photosynthetic electron transport chain are collectively known non-photochemical quenching (NPQ) mechanisms, and their induction is thought to reduce damage to the photosynthetic apparatus caused by synthesis of ROS (Demmig-Adams and Adams, 1992; Muller, 2001). As such, the scavenging/antioxidant network to remove ROS and repair damge is complex (Asada, 1999; Mullineaux et al., 2006; Miller et al., 2010). Notably, although in C_3 species such as *Arabidopsis thaliana*, mesophyll cells contain the majority of chlorophyll in a leaf, after exposure to excess light ROS accumulate preferentially in bundle sheath cells that surround veins (Fryer et al., 2002; Fryer et al., 2003; Mullineaux et al., 2006; Galvez-Valdivieso et al., 2009). ROS have been implicated in rapid systemic signaling responses initiated after various abiotic and biotic stresses including heat, wounding and pathogen attack (Fichman and Mittler, 2020). Such ROS mediated signaling from a locally perturbed leaf can lead to stomatal aperture being altered in distant leaves, is associated with the hormones abscisic and jasmonic acid, and dependent on the plasma membrane localized NADPH oxidase

77 (Respiratory Burst Oxidase Homolog D (RBOHD) (Devireddy et al., 2018; Devireddy et al.,
78 2020).

79 In contrast to C_4 species in which the role of the bundle sheath in fixing CO_2 by RuBisCO
80 has been understood for decades (Hatch, 1987), this cell-type is poorly characterized in C_3
81 species. Whilst the bundle sheath of C_3 plants contains chloroplasts that accumulate starch
82 (Miyake and Maeda, 1976; Kinsman and Pyke, 1998) they are not as numerous as those in
83 the mesophyll and reducing chlorophyll accumulation in these cells has limited impact on
84 photosynthesis (Janacek et al., 2009). Rather, in *A. thaliana* the bundle sheath is thought to
85 be specialized in sulphur metabolism, glucosinolate biosynthesis (Gigolashvili et al., 2007;
86 Koroleva et al., 2010; Aubry et al., 2014) and transport of water and solutes in and out of the
87 leaf (Aubry et al., 2014). In particular, stress responsive activation of aquaporins in bundle-
88 sheath cells are important in hydraulic conductivity of the whole leaf (Shatil-Cohen et al.,
89 2011; Sade et al., 2014; Sadey et al., 2015). Consistent with this, bundle sheath cells more
90 generally have been proposed to play a role in maintaining hydraulic integrity of the xylem
91 (Sage, 2001; Griffiths et al., 2013) and in regulating flux of metabolites in and out of the leaf
92 (Leegood, 2008).

93 To our knowledge none of these previous studies explain how the bundle sheath of C_3
94 plants preferentially accumulates ROS. One possibility is that supply of atmospheric CO_2 to
95 cells around the veins is limited and so inorganic carbon present in the transpiration stream
96 provides CO_2 to photosynthesis (Hibberd and Quick, 2002; Brown et al., 2010). If this were
97 the case, when stomata close, provision of CO_2 from veins could slow activity of the Calvin
98 Bassham Benson cycle compared with chlorophyll de-excitation in the light harvesting
99 complexes (Galvez-Valdivieso et al., 2009). Although, proximity of bundle sheath cells to
100 veins could provide an efficient mechanism to initiate systemic acclimation to high-light
101 stress (Mullineaux et al., 2006) the mechanism/s by which ROS accumulate in bundle
102 sheath cells is unclear, and to our knowledge how common this response is beyond *A.*
103 *thaliana* is not known.

104 Using rice, we show that ability of the C_3 bundle sheath to preferentially accumulate ROS
105 in response to high light is found in the monocotyledons as well as the dicotyledons. We
106 found no evidence that ROS accumulation in the C_3 bundle sheath was due to limited CO_2
107 supply, nor to production of H_2O_2 from photorespiration – in fact we detected clear ROS

accumulation in bundle sheath cells of C_4 species in which photorespiration is essentially abolished. We also found no evidence for an imbalance between transcript abundance of genes encoding components of light harvesting apparatus and the Calvin Bassham Benson cycle. However, we did find that transcripts encoding NADPH oxidases accumulate preferentially in bundle sheath cells. Pharmacological treatment to block their activity and overexpression reduced and increased accumulation of ROS in the bundle sheath of rice respectively. Although accumulation of ROS in the bundle sheath was strongest in green leaves containing light harvesting apparatus, accumulation was still detected in etiolated leaves.

117 **Results**

118 **Veins and bundle sheath cells of rice preferentially accumulate reactive oxygen**
119 **species in response to high light**

120 Rice leaves were exposed for 90 minutes to a light intensity tenfold higher than that used
121 for growth. As expected, this led to a rapid and sustained reduction in the chlorophyll
122 fluorescence parameters Fv'/Fm' and Fq'/Fm' (Figure 1A&B) that report the maximum
123 efficiency of Photosystem II and its operating efficiency respectively. Over the same period,
124 photochemical quenching first decreased and then recovered slowly, whilst non-
125 photochemical quenching increased steadily (Figure 1C). Representative images of Fv'/Fm'
126 over this time-course indicated that responses of the photosynthetic apparatus to high light
127 were relatively homogenous across the leaf (Figure 1D). Together, these data show that
128 subjecting rice leaves to excess light led to the expected response of Photosystem II
129 efficiency.

130 We next tested whether preferential accumulation of ROS in bundle sheath cells as
131 reported in *A. thaliana* (Fryer et al., 2002; Fryer et al., 2003; Galvez-Valdivieso et al., 2009)
132 was detectable in rice. The cytochemical dye 3, 3-diaminobenzidine (DAB) is routinely used
133 to detect H_2O_2. It reacts with H_2O_2 to form a brown polymerization product, the reaction
134 being accelerated by peroxidase (Thordal-Christensen et al., 1997). In contrast to the
135 relatively homogenous alterations to chlorophyll fluorescence parameters reporting on the
136 activity of Photosystem II (Figure 1D), preferential accumulation of the DAB polymerization
137 product (hereafter referred to as DAB) was detected in patches of longitudinal files of cells
138 after five minutes, and then in almost all files of these cells after thirty minutes of exposure
139 to high light (Figure 1E). Paradermal sections from leaves were generated in order to
140 determine the specific cell types involved, and this showed that thirty minutes after exposure
141 to high light the strongest DAB signal was associated with veins and bundle sheath cells
142 (Figure 1F). We refer to these cells as bundle sheath strands (BSS) as they include both the
143 bundle sheath and the vascular strands. Quantitation of this signal from multiple sections
144 confirmed that bundle sheath strands consistently accumulated more DAB than the
145 surrounding mesophyll cells (Figure 1G) and more dense sampling indicated that the
146 increase in DAB was first detectable ten minutes after the transfer to high light (Figure
147 S1A&B). From around fifteen minutes after the treatment, DAB also increased in mesophyll

148 cells, but the signal was always stronger in bundle sheath strands (Figure S1A&B). We used
149 the ROS sensitive fluorescent dye 2',7'-dichlorodihydrofluorescein diacetate (H_2DCFDA) to
150 provide independent evidence that rice bundle sheath strands were particularly responsive
151 to high light. In the presence of peroxidases and radicals generated by ROS in living plant
152 cells, H_2DCFDA produces highly fluorescent 2',7'-dichlorofluorescein (DCF) (Winterbourn,
153 2014). Consistent with the results obtained with DAB, when H_2DCFDA was supplied to rice
154 leaves, high light led to brighter green fluorescence in bundle sheath strands than
155 neighbouring cells (Figure S2A). To exclude the possibility that H_2DCFDA had not uniformly
156 penetrated mesophyll cells, we supplied a subset of leaves with exogenous H_2O_2 (Figure
157 S2B). This led to DCF fluorescence from both mesophyll as well as bundle sheath strands
158 indicating that the increased signal in the bundle sheath after exposure to high light was
159 unlikely to be an artefact of incomplete transport into all cells of the leaf (Figure S2B).
160 Localised staining also rules out direct dye oxidation by light (Winterbourn, 2014). We
161 conclude that as with *A. thaliana*, veins and bundle sheath cells of rice preferentially
162 accumulate ROS in response to high light treatment and thus that this may be a property
163 found in both dicotyledons and monocotyledons.
164

165 **Over-capacity in light harvesting compared with Calvin-Benson-Bassham cycle**
166 **capacity is unlikely the cause of DAB accumulation in rice bundle sheath strands**

167 Excess excitation energy that cannot be fully utilized by carbon assimilation and other
168 metabolic processes in chloroplasts gives rise to ROS during exposure to high light intensity
169 (Fryer et al., 2003; Apel and Hirt, 2004; Bechtold et al., 2008). The greater production of
170 ROS in the BSS compared with mesophyll cells implies a greater capacity for ROS
171 production or a limitation imposed by CO_2 assimilation rate. As bundle sheath strands are
172 distant from stomata, and in contact with fewer intercellular air spaces than mesophyll cells,
173 we reasoned that they may be CO_2 limited. Thus, flux through the Calvin-Benson-Bassham
174 cycle may be constrained compared with activity of the photosynthetic electron transport
175 chain. If this were the case, reducing and increasing the CO_2 concentration around leaves
176 would be expected to respectively enhance and repress preferential DAB staining in bundle
177 sheath strands. However, we found evidence for neither. High light exposure at 200 ppm
178 [CO_2], which would restrict activity of the Calvin Benson Bassham cycle, led to preferential

179 but similar DAB staining in the bundle sheath strands and 2000 ppm [CO_2], which should
180 saturate RuBisCO in bundle sheath as well as mesophyll cells, failed to abolish the
181 preferential DAB staining in these cells (Figure 2A&B).

182 The oxygenation reaction of RuBisCO requires the photorespiratory pathway to detoxify
183 the initial product phosphoglycolate, and in so doing H_2O_2 is released by glycolate oxidase
184 in peroxisomes. It is therefore possible that rapid DAB staining in bundle sheath strands is
185 due to high rates of photorespiration in this cell type. To test this, we reduced the oxygen
186 tension to 2%, but found that this had no clear effect on DAB staining compared with controls
187 (Figure 3A&B). Moreover, when leaves of the C_4 species *Gynandropsis gynandra, Setaria*
188 *italica, Zea mays* and *Sorghum bicolor*, which generate up to tenfold higher concentrations
189 of CO_2 in bundle sheath cells and therefore minimal activities of photorespiration were
190 exposed to high light, DAB still accumulated in these cells over a similar time-course (Figure
191 3C). It therefore appears unlikely that preferential DAB staining in either C_3 or C_4 bundle
192 sheath cells is caused by H_2O_2 produced during photorespiration.

193 Taken together our results imply that accumulation of ROS in the bundle sheath of C_3
194 and C_4 plants is unlikely to be caused by limited capacity of the Calvin-Benson-Bassham
195 cycle compared with ability to harvest light energy. Furthermore, the data obtained by
196 suppressing photorespiration either transiently in C_3 leaves, or more permanently in C_4
197 leaves, are inconsistent with the notion that photorespiratory derived H_2O_2 is responsible for
198 the rapid accumulation of ROS in bundle sheath cells.

199

200 **Transcriptome profiling indicates balanced expression of photosynthesis genes but**
201 **elevated expression of genes encoding enzymes responsible for synthesis of reactive**
202 **oxygen species in bundle sheath strands**

203 To better understand the molecular basis for preferential accumulation of ROS in rice
204 bundle sheath strands we carried out RNA-SEQ on this tissue. Laser capture
205 microdissection was used to obtain mRNA from three biological replicates of bundle sheath
206 strands or mesophyll cells derived from leaves that had not received a high light treatment
207 (Figure 4A). Electropherograms showed that the RNA obtained was of good quality (Figure
208 4B). In total, over 165 million reads were generated using the Illumina sequencing platform.
209 For each replicate, on average about 78.5% of reads were mapped uniquely to the

210 Nipponbare reference genome (Supplemental Table 1). To enable comparison between
211 samples, we normalized all read counts with DESeq2, and to reduce noise, poorly
212 expressed genes with averaged normalized counts of < 10 in all samples were removed.
213 This led to a total of 15,727 genes being identified as expressed. Among these, 15456 genes
214 were expressed in both BSS and M cells, while 239 genes were only expressed in BSS and
215 32 genes only expressed in M cells (Figure 4C). Hierarchical clustering (Figure 4D) and
216 principal component analysis (PCA; Figure 4E) showed strong clustering between biological
217 replicates from each tissue. Indeed, the PCA showed that 92% of variance between
218 replicates was associated with one major component that mapped onto the tissue from
219 which RNA was isolated (Figure 4E). Using criteria of $\log_2$ fold change > 0.5 and an adjusted
220 *P* value < 0.05, we defined 3170 genes as being more highly expressed in bundle sheath
221 strands, and 2766 as more strongly expressed in mesophyll cells (Figure 4F).

222 We next analysed the abundance of transcripts derived from genes known to be
223 associated with the production of ROS. Specifically, we focused on genes encoding the
224 photosynthetic apparatus, and enzymes that either scavenge or synthesize ROS. In all
225 cases, to provide an overview of these complex processes eigengene values were
226 computed to take into account the fact that multiple genes encode these oligomeric protein
227 complexes. Transcripts encoding components of Photosystem II, Photosystem I, the
228 cytochrome b_6f complex, cyclic electron transport and the ATP synthase were less abundant
229 in bundle sheath strands compared with mesophyll cells (Figure 4G and Figure S3).
230 However, the mesophyll contains a larger chloroplast compartment (Kinsman and Pyke,
231 1998) and so this is to be expected. We thus normalized transcript abundance for each
232 complex to Photosystem II and Photosystem I (Figure S3). This showed that components of
233 Photosystem II, the cytochrome b6f complex and Photosystem I accumulated
234 stoichiometrically in both cell types (Figure 4G). In other words, there was no clear
235 imbalance in transcripts encoding one part of the photosynthetic electron transport chain
236 that might lead to impaired function. This was also true for transcripts encoding enzymes of
237 the Calvin-Benson-Bassham cycle (Figure 4G) indicating that the relative capacities of the
238 light-dependent reactions of photosynthesis and the Calvin-Benson-Bassham cycle are
239 balanced similarly in bundle sheath strands and mesophyll cells. These data are consistent
240 with our earlier finding that increasing the CO_2 concentration around leaves failed to abolish

241 accumulation of DAB staining in the rice bundle sheath (Figure 2A&B).

242 We also found no evidence from this analysis of transcript abundance that bundle sheath
243 strands have lower ability to detoxify ROS than the mesophyll (Figure 4H). After
244 normalization to transcripts for the Photosystems which would be an expected source of
245 ROS during high light stress, transcripts encoding enzymes known to scavenge ROS were
246 typically more abundant in bundle sheath strands compared with mesophyll cells (Figure
247 4H). However, transcripts encoding several NADPH-oxidase and superoxide dismutase
248 proteins, which generate superoxide and H_2O_2 respectively were more abundant in bundle
249 sheath strands compared with mesophyll cells (Figure 4I). In particular, transcripts encoding
250 RBOHA, RBOHC and RBOHI were considerably more abundant in bundles sheath strands
251 compared with mesophyll cells. Quantitative Polymerase Chain Reactions (Q-PCR)
252 confirmed these findings (Figure S4). These data imply that the rapid increase in ROS in
253 bundle sheath strands after exposure to high-light is unlikely associated with a limited ability
254 to dissipate energy associated with the photosynthetic electron chain, but rather appears
255 due to higher basal activities of proteins that synthesize ROS.

256

257 **NADPH-oxidase activity mediates the high light response in both green and etiolated**
258 **leaves**

259 To test whether NADPH-oxidase activity is important for ROS accumulation in bundle
260 sheath strands of rice we used inhibitors to block its activity, as well as a previously reported
261 overexpression line for the *OsRBOHA* gene that encodes the major RBOH isoform NADPH-
262 oxidase A in rice (Wang et al., 2016). Two commonly employed inhibitors of flavin-linked
263 enzymes, diphenyleneiodonium chloride (DPI) (O'Donnell et al., 1993) and imidazole (Iizuka
264 et al., 1985), were used to assess the role of NADPH oxidase. Both inhibitors reduced ROS
265 production in bundle sheath strands of rice after imposition of light stress (Figure 5A&B and
266 Figure S5A&B). The incomplete repression of ROS production associated with DPI or
267 imidazole treatment is consistent with some production being associated with
268 photosynthesis-related processes. To test whether this was the case, we next exposed
269 etiolated leaves that lack chlorophyll to high light in the absence or presence of each inhibitor.
270 Despite these leaves lacking chlorophyll, DAB staining was detected after exposure to high-
271 light (Figure 5C&D, Figure S5C&D). This is consistent with a significant amount of ROS

being produced from non-photosynthetic pathways. Moreover, in leaves lacking chlorophyll, inhibition of NADPH-oxidase activity completely abolished ROS production in bundle sheath strands (Figure 5C&D, Figure S5C&D). Q-PCR on RNA isolated from etiolated leaves confirmed that transcripts derived from *NADPH-oxidase A*, *NADPH-oxidase* C and *NADPH-oxidase I* genes as well as superoxide dismutase genes were more abundant in bundle sheath strands than in mesophyll cells (Figure S6). Whilst a mutant allele for *NADPH-oxidase B*, which was preferentially expressed in mesophyll cells (Figure 4I) had no impact on DAB staining during high light treatment (Figure S7), leaves from an overexpressor of *NADPH-oxidase A* (Wang et al., 2016) showed increased DAB staining in rice bundle sheath strands compared with controls (Figure 5E&F and Figure S8). We thus conclude that *NADPH-oxidase A* is important in mediating the response to high light in bundle sheath strands of rice.

284 **Discussion**

285 In the C_3 species *A. thaliana* it has been known for some time that bundle sheath cells
286 accumulate ROS in response to excess light (Fryer et al., 2002; Fryer et al., 2003;
287 Mullineaux et al., 2006; Galvez-Valdivieso et al., 2009). The work presented here shows that
288 a similar response is detected in bundle sheath strands of rice, a C_3 species from the
289 monocotyledons. Moreover, our analysis indicates that this phenomenon is not associated
290 with C_3 photosynthesis, but that it also takes place in bundle sheath strands from leaves of
291 C_4 plants. This was the case in C_4 *Gynandropsis gynandra*, which is sister to the
292 Brassicaceae, but also in the C_4 grasses maize, sorghum and *Setaria*. These findings imply
293 that the bundle sheath from dicotyledons and monocotyledons of both C_3 and C_4 species
294 fulfills a role in sensing and responding to excess light.

295 To better understand the causes for production of ROS in bundle sheath strands we used
296 rice. High light-induced ROS was not abolished by decreasing photorespiration in rice and
297 could be seen in the bundle sheath strands of C_4 species that lack photorespiration.
298 Therefore, photorespiratory H_2O_2 production in peroxisomes *via* glycolate oxidase is not
299 involved. The possibility that an imbalance between light harvesting and photosynthetic
300 electron transport and use of excitation energy by the Calvin-Benson-Bassham cycle in
301 bundle sheath cells was not supported by relative expression of genes encoding
302 photosynthetic components. After normalization, these have similar relative expression in
303 both cell types. This finding is consistent with analysis of the bundle sheath in C_3 *A. thaliana*
304 in which the photosynthetic apparatus is assembled and functional (Kinsman and Pyke,
305 1998; Janacek et al., 2009) despite lower levels of photosynthesis gene expression (Aubry
306 et al., 2014). We also failed to collect any convincing physiological evidence that ROS
307 production in the rice bundle sheath was associated with restricted activity of the Calvin-
308 Benson-Bassham cycle as might be expected if provision of CO_2 to this tissue distant from
309 stomata was limiting. The accumulation of ROS was neither accentuated nor ameliorated
310 when intercellular CO_2 concentrations were reduced or increased respectively.

311 In contrast to a purely photosynthetic origin of ROS in bundle sheath strands, we have
312 produced evidence that plasma membrane localized NADPH oxidase has a significant role.
313 NADPH oxidase catalyses extracellular reduction of oxygen, forming superoxide in the
314 apoplast. Membrane impermeable superoxide dismutates rapidly, producing H_2O_2 which is

315 proposed to enter the cytosol through aquaporins. NADPH oxidase has numerous isoforms
316 and is activated rapidly following numerous stimuli (Smirnoff and Arnaud, 2019). There is
317 evidence for apoplastic ROS production in *A. thaliana* bundle sheath cells in response to
318 high light (Galvez-Valdivieso et al., 2009) although NADPH depdendence was not
319 established. We found that three NADPH oxidase isoforms (RBOHA, RBOHC and RBOHI)
320 were more highly expressed in rice bundle sheath strands compared with mesophyll cells.
321 Consistent with NADPH oxidase being involved, application of the flavoprotein inhibitors
322 (DPI and imidazole) removed a large proportion of HL-induced ROS production. Moreover,
323 a mutant allele and overexpressing line for *OsRBOHB*, which was more abundant in
324 mesophyll cells showed no effect on ROS accumulation, whilst overexpression plants for
325 *OsRBOHA* led to increased production of ROS in the bundle sheath. Thus, differential
326 transcript abundance between the cell-types, pharmacological approaches to inhibit NADPH
327 oxidase activity, and genetic perturbation of the *OsRBOHA* locus supported the notion that
328 the bundle sheath strands have a greater ability than mesophyll cells to synthesize ROS in
329 response to high light. Furthermore, the observation that etiolated leaves have high light
330 induced ROS production provides key evidence that it is independent of photosynthesis and
331 supports a role for NADPH oxidase. How NADPH oxidase is activated by light in etiolated
332 leaves will need to be determined in the future. One possibility could be photoreceptor-
333 mediated NADPH oxidase activation. Cryptochrome generates superoxide upon exposure
334 to blue light and this has been proposed to contribute to part of its signaling role (El-Esawi
335 et al., 2017). However, it is also possible that photoreceptors could activate NADPH oxidase.
336 The results also suggest that part of the light-induced ROS derive from photosynthesis.
337 Given that previous work has shown that chloroplasts release H_2O_2 in the light and that this
338 could provide a high light signaling mechanism (Exposito-Rodriguez et al., 2017; Smirnoff
339 and Arnaud, 2019), the possible differences in the function of chloroplast and NADPH
340 oxidase-derived ROS requires investigation.

341 NADPH oxidase has previously been implicated in ROS responses induced by biotic and
342 abiotic stresses. In response to a localized stress event, an NADPH oxidase-dependent
343 ROS wave propagates between cells to initiate systemic responses in tissues distant from
344 the original stress (Miller et al., 2010; Mittler et al., 2011; Zandalinas and Mittler, 2018;
345 Fichman et al., 2019). Whilst we did not aim to investigate components underpinning such

346 a wave, or downstream responses, our findings have some relevance to the role of NADPH
347 oxidase in ROS production. The data imply that rice *RBOHA* plays a role in a local production
348 of ROS in bundle sheath strands. How these findings relate to previous work on *A. thaliana*
349 will require further work. The gene families encoding these proteins are large, and the
350 phylogenetic distance between *A. thaliana* and rice means that direct orthologs are not
351 always found, and function of these proteins may have diverged. However, *RBOHA* from
352 rice, which appears to play an important role ROS accumulation in the bundle sheath in
353 response to high light, is in the same orthogroup as *RBOHF* from *A. thaliana* (Figure S9A).
354 Interestingly, compared with the whole leaf, transcripts of *AtRBOHF* were more abundant in
355 bundle sheath cells (Figure S9B; (Aubry et al., 2014)). Thus, it is possible that these
356 orthologs fulfill similar functions in the bundle sheath strands of both species. However,
357 several lines of evidence point towards multiple pathways that both synthesize and
358 propagate ROS production in response to stresses. For example, analysis of *A. thaliana*
359 reported production of ROS in bundle sheath strands in leaves subjected to high light stress
360 (Fryer et al., 2002; Fryer et al., 2003; Mullineaux et al., 2006; Galvez-Valdivieso et al., 2009),
361 whilst in distant leaves ROS production is preferentially detected in mesophyll cells
362 (Fichman et al., 2019; Fichman and Mittler, 2020). Moreover, differential changes in stomatal
363 aperture of leaves subjected to stress compared with distant non-stressed leaves support a
364 model in which two different signals are involved in systemic stomatal responses. One that
365 is ABA based and associated with the vascular system (Schachtman and Goodger, 2008;
366 KangasjÄrvi et al., 2009; Gorecka et al., 2014; Yoshida and Fernie, 2018) and another that
367 uses ROS and travels through the plant (Devireddy et al., 2020). In fact, after a dark to light
368 transition in *A. thaliana*, local changes to stomatal aperture were not dependent on *RBOHD*,
369 but those changes associated with the systemic response were. *RBOHD* from *A. thaliana* is
370 orthologous to *RBOHI* from rice and in both species transcripts appear to be more abundant
371 in bundle sheath strands (Figure S9C&D and (Aubry et al., 2014)). This finding implies that
372 the role of these two proteins may have been conserved since they diverged from the last
373 common ancestor of rice and *A. thaliana*. Thus, downstream effects of production of ROS
374 in the bundle sheath will require additional experimentation. One important advance in this
375 area has been the ability to non-invasively monitor ROS either with reporters such as Hyper2
376 and roGFP (Exposito-Rodriguez et al., 2017; Nietzel et al., 2019), or with addition of

fluorescent dyes to intact leaves to allow time-course analysis in locally stressed as well as distantly responding tissues (Fichman et al., 2019). Being able to apply these non-invasive approaches to tissues such as the bundle sheath that are deep in the leaf and therefore challenging to image will be informative in the future.

381 **Materials and methods**

382 **Plant materials and high light stress**

383 Rice (*Oryza sativa*. L) plants were grown for two weeks in compost in a growth chamber
384 with a 16 h photoperiod with a photosynthetic photon flux density (PPFD) of 75 µmol m^{-2} s^{-}
385 ^{1}, day night temperatures of 28 and 26°C respectively, and relative humility of 60%. In all
386 experiments, unless otherwise stated, IR64 was used. *OsRBOHA* and *OsRBOHB*
387 overexpression lines and *Osrbohb* mutants as well as their background (Nipponbare), were
388 grown under the same conditions. Etiolated plants were obtained by growing the plants in
389 compost in the dark at 28/26°C for 2 weeks.

390 In all cases, the middle part (~2.5 cm) of the second leaf was taken and infiltrated with
391 dye solution (see below). Leaves were then subjected to 750 µmol m^{-2} s^{-1}, which represented
392 a tenfold increase above that of growth. High light was provided using a Clark-type oxygen
393 electrode (LD2/3 oxygen electrode chamber) connected to an Oxylab control unit
394 (Hansatech Instruments Ltd., Norfolk, UK) and temperature maintained at 28°C using a
395 water tank. The top half of the leaves were illuminated by a liquid electronic display (LED)
396 light source (Hansatech LH36-2), whilst the bottom half of the leaf was covered with tin foil
397 to keep it in the dark.

398

399 **Chlorophyll fluorescence imaging**

400 Chlorophyll fluorescence measurements were performed using a chlorophyll fluorescent
401 imaging system (CF Imager, Technologica Ltd, Colchester, UK). ~ 2 cm leaf strips of the
402 middle part of second leaves were detached and floated on water in a 25-well square dish
403 and transferred immediately into the CF Imager. The application of pre-programmed
404 regimes of actinic growth light exposure times, dark periods, saturating light pulses, and the
405 calculation and imaging of the parameters F_v/F_m, F_q'/F_m', F_v'/F_m', and NPQ (Baker, 2008)
406 were performed using the manufacturers software-FluorImager.

407

408 **Detection of reactive oxygen species**

409 H_2O_2 production in the cells was detected by staining with 3,3'-diaminobenzidine
410 tetrachloride (DAB) (Fryer et al., 2002; Driever et al., 2009). The middle 2 cm from second
411 leaves were soaked in 5 mM DAB solution (pH 5.0) with 0.01% Tween-20. After shaking in

412 a dark incubator at 28°C for 2 hours, leaves were briefly dried with tissue paper, placed in a
413 Hansatech LD2/ 3 electrode leaf chamber and subjected to 750 μmol m^{-2} s^{-1}. Sampling was
414 undertaken at 0, 5, 10, 15, 20, 30, 40, 50, 60 mins. Prior to imaging, chlorophyll was removed
415 from the leaves by soaking in ethanol:acetic acid:glycerol (3:1:1) in a 70°C water bath for 1
416 hour, and then immersing in 70% (v/v) ethanol for 24 hours.

417 H_2O_2 production was also detected with 2',7'-dichlorodihydrofluorescein diacetate
418 (H_2DCFDA, Sigma-Aldrich). H_2DCFDA was dissolved in dimethyl sulfite (DMSO) to 20 mM,
419 and then diluted with H_2O to a final concentration of 10 μM for infiltration. Infiltration was
420 performed as previously described (Fryer et al., 2002; Driever et al., 2009). In short,
421 H_2DCFDA was fed through the transpiration stream under low light (20 μmol m^{-2} s^{-1}) for up
422 to 12 hours to ensure absorption throughout the leaf. After infiltration, leaves were then
423 clamped in the Hansatech LD2/3 electrode chamber and exposed to PPFD of 750 μmol m^{-}
424 ^{2} s^{-1} for 0, 30, 60 minutes. Prior to confocal laser scanning microscopy, the middle vein of
425 the leaf was imaged after generating a paradermal section by hand. To confirm whether
426 H_2DCFDA penetrated into the whole leaf, 30% (w/w) H_2O_2 solution was diluted to 100 mM
427 with 10 μM H_2DCFDA and used to infiltrate leaves under the same conditions as above.
428 Leaves infiltrated with ddH_2O at the same condition were used as controls. After infiltration,
429 green fluorescence was assessed by confocal laser scanning microscopy.

430 The NADPH oxidase inhibitors diphenyliodonium (DPI) and imidazole (Sigma) were
431 added to the DAB solution and infiltrated into leaves for 2 hours before high light treatment.
432 DPI chloride was dissolved in DMSO to 100 mM and then diluted to 100 μM with a 5 mM
433 DAB solution (pH 5.0, with 0.01% tween20). Imidazole was dissolved in DMSO to 1 mM and
434 then diluted with 5 mM DAB solution (pH 5.0, with 0.01% tween20) to 20 μM. To test the
435 effects of different CO_2 and O_2 contents on H_2O_2 products, DAB-infiltrated leaves were
436 subjected to the high light treatment as described above, using air mixtures with different
437 concentrations of CO_2 controlled by an open gas exchange analyzer (LI-6400, LI-COR
438 Biosciences, Lincoln, NE, USA) connected in line to the Hansatech LD2/ 3 electrode leaf
439 chamber. For measurements at 2% O_2 concentration, the LI-6400 air inlet was connected
440 to a gas cylinder with pre-mixed 2% O_2 in N_2.
441

442 **Paradermal sectioning of paraffin-embedded tissue**

443 Leaves used for paradermal sectioning had been treated with high light and chlorophyll
444 removed. Samples were cut into small pieces of ~ 5 mM and dehydrated in an ethanol series
445 consisting of 70% (v/v) for 30 minutes; 85% (v/v) for 30 minutes; 95% (v/v) for 30 minutes;
446 100% (v/v) ethanol twice for 30 minutes, then twice in 100% (v/v) Histo-Clear II for 60
447 minutes each, followed by two times in paraffin wax for 60 minutes at 60°C. Melted paraffin
448 wax was poured into 9-cm petri dishes and cut into small blocks once the wax was cool. For
449 paradermal sectioning, blocks were trimmed so that the surface of the leaf was parallel to
450 the surface of the block. 10 µm sections were obtained using a rotary microtome, floated in
451 a 60°C water bath and then mounted onto clean glass slides to dry overnight in an incubator
452 set at 42°C. Dehydration of the sections was performed as follows: 100% (v/v) Histo-Clear
453 II twice for 10 minutes each; 100% ethanol twice for 5 minutes each; 95% ethanol (v/v); 70%
454 (v/v) ethanol; 50% (v/v) ethanol; 30% (v/v) ethanol for 2 minutes each. Slides were then
455 rinsed with deionized H_2O; drained and then 30% (v/v) glycerol added prior to a coverslip.

456

457 **Laser capture microdissection**

458 For laser capture microdissection, leaf samples were cut into ~ 5 mm pieces and fixed in
459 100% (v/v) ice-cold acetone at 4°C for overnight. The next day, samples were dehydrated
460 and embedded with Steedman's polyester wax (Hua and Hibberd, 2019). Blocks were
461 sectioned using a rotary microtome to 8 µm thickness and then floated on Arcturus PEN
462 membrane slides (Fisher Scientific) with DEPC-treated water. The water was dried using
463 tissue paper and slides were stored at -20°C and used within 12 hours after sectioning. Prior
464 to LCM, slides were washed in 100% (v/v) ethanol for 5 mins and then air-dried for 5 mins.
465 LCM was performed using the ArcturusXT™ Laser Capture Microdissection System
466 (ThermoFisher) according to the manufacturer's instructions. Mesophyll cells and bundle
467 sheath stands were collected on the CapSure® Macro LCM Caps (ThermoFisher) and
468 immediately treated with extraction buffer (from Arcturus Picopure RNA extraction kit
469 (Thermo Fisher Scientific)) at 42°C for 30 minutes, then stored at -80°C.

470

471 **RNA extraction and quantitative PCR (qRT-PCR)**

472 Total RNA from LCM harvested mesophyll and bundle sheath cells was extracted using

473 Arcturus Picopure RNA extraction kit (ThermoFisher) with on-column DNaseI treatment
474 according to the manufacturer's protocol. cDNA synthesis for LCM samples was performed
475 using TruSeq RNA Library Preparation Kit v2 (RS-122-2001; Illumina). Total RNA from
476 whole leaves was extracted from 100 to 200 mg of fully expanded leaves using Triazol
477 reagent (Sigma-Aldrich) according to the manufacturer's instructions. Superscript II reverse
478 transcriptase (18064-022; ThermoFisher Scientific) was used for cDNA synthesis of whole
479 leaves. qRT–PCR was performed with the Bio-Rad CFX384 Real-Time PCR system using
480 the SYBR Green Jumpstart Taq ReadyMix (S4438-100RXN; Sigma-Aldrich) with the
481 following PCR conditions: 94°C for 5 mins and 40 cycles of 94°C for 10 s, 60°C for 1 min.
482 Relative gene expression levels were calculated using the $2^{-\Delta\Delta CT}$ method (Kubista et al.,
483 2006) and normalized with *OsUBQ5.* Gene-specific primer sequences are listed in
484 Supplemental Table 2. For each gene, three biological and three technical replicates were
485 performed.
486
487 **RNA-sequencing library preparation and data processing**
488 RNA integrity and quality of LCM samples were assessed using 2100-Bioanalyzer
489 (Agilent Technologies, USA) with an Agilent Bioanalyser RNA 6000 Pico assay and QuBit
490 (Thermo Fisher Scientific), respectively. Only samples RNA Integrity Number (RIN) ≥4.4
491 were selected for the final sample cohort. 50~150 ng starting total RNA from 12~15
492 paradermal sections of each replicate were used for RNA-seq library construction using the
493 QuantSeq 3' mRNA-Seq Library Prep Kit (Lexogen) according to the manufacturer's
494 recommendations. cDNA libraries were assessed using 2100-Bioanalyzer (Agilent
495 Technologies, USA) before 100 bp single-end sequencing using NextSeq500 (Illumina)
496 system at the Department of Biochemistry Sequencing Services at the University of
497 Cambridge based on standard protocols. Three biological replicates were conducted for
498 each cell type. Data processing was performed using custom scripts. Briefly, raw reads were
499 processed using Trimmomatic, mapped to the reference rice transcriptome genome
500 (MSU7.0, http://rice.plantbiology.msu.edu/index.shtml) and performed quantified using
501 Salmon (Patro et al., 2017). Differential expression analysis was performed using DESeq2.
502 Stringent criteria with $\log_2$ fold change ($\log_2$FC) >0.5 and adjusted p value (padj) < 0.05 were
503 used to screen the differentially expressed genes (DEGs) between bundle sheath strand

504 and mesophyll cells. Plots were generated with custom scripts in RStudio using the package
505 ggplot2. Three biological replicates for each cell type were performed.
506
507 **Generation of *OsRBOHB*-overexpression (*OsRBOHB*-OE) lines**
508 To generate the *OsRBOHB*-OE plants, the full-length coding region of *OsRBOHB* was
509 was amplified from the first-strand cDNA of Nipponbare and insert into vector pCAMBIA1301
510 under the control of ubiquitin promoter. The resulted construct was transformed into
511 Nipponbare by Agrobacterium-mediated transformation. The primers used for the construct
512 are listed in Supplemental Table 2.
513
514 **Imaging**
515 Intact leaves were imaged with Leica m165 FC microscopy. The paradermal sections
516 were imaged with Olympus BX41 microscopy. DAB staining intensity was quantified using
517 ImageJ (FIJI build, version 1.52q, NIH, USA). Confocal micrographs for detecting the DCF
518 fluorescence were taken using a Leica SP8 confocal microscopy (excitation 488 nm, barrier
519 515–555 nm).
520
521 **Statistical analysis**
522 All statistical analyses were conducted in R (v.3.6.3). Two-way analysis of variance
523 (ANOVA) was used to assess statistical differences in DAB staining between BSS and M
524 cells after a time course of high light treatment, and the effects of different concentrations of
525 CO_2 and O_2 concentrations on H_2O_2 production under high light treatment. Three-way
526 ANOVA was used for statistical analysis on the effects of different concentrations of CO_2 and
527 O_2 concentrations on H_2O_2 production under high light treatment and also used for assess
528 the data in experiments with the inhibitors DPI, imidazole, and also used to compare the
529 H_2O_2 production of *OsRBOHA*-OE and its wildtype under a time course of high light
530 treatment. Tukey Honest Significant Differences (TukeyHSD) test was performed for multiple
531 pairwise-comparison between the means of groups. Levene's test was used to check the
532 homogeneity of variances and Shapiro-Wilk test was used to check the normality
533 assumption. Unpaired T-tests were performed to compare differences in transcript
534 abundance between BSS and M cells and also used to compare the differences in DAB

535 staining between wild type and *OsRBOHB*-overexpression lines and mutants under
536 dark/high light conditions.
537

538 **Acknowledgements**

539 We thank Ivan Reyna-Llorens (University of Cambridge) for making the phylogenetic tree.
540 The work was funded by China International Postdoctoral Exchange Fellowship to HX, ERC
541 grant RG80867 Revolution to JMH and a C_4 Rice project grant from The Bill and Melinda
542 Gates Foundation to the University of Oxford (2015–2019).
543

544 **Competing interests**

545 The authors declare that they have no competing interests.

546 **References**

547 **Apel K, Hirt H** (2004) REACTIVE OXYGEN SPECIES: Metabolism, Oxidative Stress, and
548 Signal Transduction. Annu Rev Plant Biol **55**: 373–399

549 **Asada K** (1999) THE WATER-WATER CYCLE IN CHLOROPLASTS: Scavenging of Active
550 Oxygens and Dissipation of Excess Photons. Annu Rev Plant Physiol Plant Mol Biol **50**:
551 601–639

552 **Aubry S, Smith-Unna RD, Boursnell CM, Kopriva S, Hibberd JM** (2014) Transcript
553 residency on ribosomes reveals a key role for the Arabidopsis thaliana bundle sheath
554 in sulfur and glucosinolate metabolism. Plant J **78**: 659–673

555 **Baker NR** (2008) Chlorophyll fluorescence: a probe of photosynthesis in vivo. PG - 89-113
556 LID - 10.1146/annurev.arplant.59.032607.092759 [doi]. Annu Rev Plant Biol 89–11

557 **Bechtold U, Richard O, Zamboni A, Gapper C, Geisler M, Pogson B, Karpinski S,**
558 **Mullineaux PM** (2008) Impact of chloroplastic- and extracellular-sourced ROS on high
559 light-responsive gene expression in Arabidopsis. J Exp Bot **59**: 121–133

560 **Brown NJ, Palmer BG, Stanley S, Hajaji H, Janacek SH, Astley HM, Parsley K, Kajala**
561 **K, Quick WP, Trenkamp S, et al** (2010) C4 acid decarboxylases required for C4
562 photosynthesis are active in the mid-vein of the C3 species Arabidopsis thaliana, and
563 are important in sugar and amino acid metabolism. Plant J **61**: 122–133

564 **Crisp PA, Ganguly D, Smith AB, Murray KD, Estavillo GM, Searle IR, Ford E,**
565 **Bogdanović O, Lister R, Borevitz JO, et al** (2017) Rapid recovery gene
566 downregulation during excess-light stress and recovery in Arabidopsis. Plant Cell **29**:
567 tpc.00828.2016

568 **Demmig-Adams B, Adams WW** (1992) Responses of plants to high light stress. Annu Rev
569 Plant Physiol Plant Mol Biol **43**: 599–626

570 **Devireddy AR, Arbogast J, Mittler R** (2020) Coordinated and rapid whole-plant systemic
571 stomatal responses. New Phytol **225**: 21–25

572 **Devireddy AR, Zandalinas SI, Gómez-Cadenas A, Blumwald E, Mittler R** (2018)
573 Coordinating the overall stomatal response of plants: Rapid leaf-to-leaf
574 communication during light stress. Sci Signal. doi: 10.1126/scisignal.aam9514

575 **Dietz KJ** (2015) Efficient high light acclimation involves rapid processes at multiple
576 mechanistic levels. J Exp Bot **66**: 2401–2414

577 **Driever SM, Fryer MJ, Mullineaux PM, Baker NR** (2009) Imaging of reactive oxygen
578 species in vivo. Methods Mol Biol **479**: 109–116
579 **Dunand C, Crèvecoeur M, Penel C** (2007) Distribution of superoxide and hydrogen
580 peroxide in Arabidopsis root and their influence on root development: Possible
581 interaction with peroxidases. New Phytol **174**: 332–341
582 **El-Esawi M, Arthaut L-D, Jourdan N, d'Harlingue A, Link J, Martino CF, Ahmad M** (2017)
583 Blue-light induced biosynthesis of ROS contributes to the signaling mechanism of
584 Arabidopsis cryptochrome. Sci Rep **7**: 13875
585 **Exposito-Rodriguez M, Laissue PP, Yvon-Durocher G, Smirnoff N, Mullineaux PM**
586 (2017) Photosynthesis-dependent H2O2 transfer from chloroplasts to nuclei provides a
587 high-light signalling mechanism. Nat Commun **8**: 1–10
588 **Fichman Y, Miller G, Mittler R** (2019) Whole-Plant Live Imaging of Reactive Oxygen
589 Species. Mol Plant **12**: 1203–1210
590 **Fichman Y, Mittler R** (2020) Rapid systemic signaling during abiotic and biotic stresses: is
591 the ROS wave master of all trades? Plant J. doi: 10.1111/tpj.14685
592 **Fryer MJ, Ball L, Oxborough K, Karpinski S, Mullineaux PM, Baker NR** (2003) Control
593 of Ascorbate Peroxidase 2 expression by hydrogen peroxide and leaf water status
594 during excess light stress reveals a functional organisation of Arabidopsis leaves. Plant
595 J **33**: 691–705
596 **Fryer MJ, Oxborough K, Mullineaux PM, Baker NR** (2002) Imaging of photo-oxidative
597 stress responses in leaves. J Exp Bot **53**: 1249–1254
598 **Galvez-Valdivieso G, Fryer MJ, Lawson T, Slattery K, Truman W, Smirnoff N, Asami T,**
599 **Davies WJ, Jones AM, Baker NR, et al** (2009) The high light response in arabidopsis
600 involves ABA signaling between vascular and bundle sheath cells W. Plant Cell **21**:
601 2143–2162
602 **Gigolashvili T, Yatusevich R, Berger B, Müller C, Flügge U-I** (2007) The R2R3-MYB
603 transcription factor HAG1/MYB28 is a regulator of methionine-derived glucosinolate
604 biosynthesis in Arabidopsis thaliana. Plant J **51**: 247–261
605 **Gorecka M, Alvarez-Fernandez R, Slattery K, Mcausland L, Davey PA, Karpinski S,**
606 **Lawson T, Mullineaux PM** (2014) Abscisic acid signalling determines susceptibility of
607 bundle sheath cells to photoinhibition in high light-exposed Arabidopsis leaves. Philos

608 Trans R Soc B Biol Sci. doi: 10.1098/rstb.2013.0234
609 **Griffiths H, Weller G, Toy L, Dennis R** (2013) You're so vein: Bundle sheath physiology,
610 phylogeny and evolution in C3 and C4 plants. Plant Cell Environ **36**: 249–261
611 **Hatch MD** (1987) C4 photosynthesis: a unique elend of modified biochemistry, anatomy and
612 ultrastructure. Biochim Biophys Acta - Rev Bioenerg **895**: 81–106
613 **Hibberd JM, Quick WP** (2002) Characteristics of C4 photosynthesis in stems and petioles
614 of C3 flowering plants. Nature **415**: 451–454
615 **Hua L, Hibberd JM** (2019) An optimized protocol for isolation of high-quality RNA through
616 laser capture microdissection of leaf material. Plant direct **3**: e00156–e00156
617 **Iizuka T, Kanegasaki S, Makino R, Tanaka T, Ishimura Y** (1985) Pyridine and imidazole
618 reversibly inhibit the respiratory burst in porcine and human neutrophils: evidence for
619 the involvement of cytochrome b558 in the reaction. Biochem Biophys Res Commun
620 **130**: 621–626
621 **Janacek SH, Trenkamp S, Palmer B, Brown NJ, Parsley K, Stanley S, Astley HM, Rolfe**
622 **SA, Paul Quick W, Fernie AR, et al** (2009) Photosynthesis in cells around veins of the
623 C(3) plant Arabidopsis thaliana is important for both the shikimate pathway and leaf
624 senescence as well as contributing to plant fitness. Plant J **59**: 329–343
625 **KangasjÄrvi S, Nurmi M, Tikkanen M, Aro EM** (2009) Cell-specific mechanisms and
626 systemic signalling as emerging themes in light acclimation of C3 plants. Plant, Cell
627 Environ **32**: 1230–1240
628 **Kimura M, Yamamoto YY, Seki M, Sakurai T, Sato M, Abe T, Yoshida S, Manabe K,**
629 **Shinozaki K, Matsui M** (2003) Identification of Arabidopsis genes regulated by high
630 light-stress using cDNA microarray. Photochem Photobiol **77**: 226–233
631 **Kinsman EA, Pyke KA** (1998) Bundle sheath cells and cell-specific plastid development in
632 Arabidopsis leaves. Development **125**: 1815–1822
633 **Kleine T, Kindgren P, Benedict C, Hendrickson L, Strand A** (2007) Genome-Wide Gene
634 Expression Analysis Reveals a Critical Role for CRYPTOCHROME1 in the Response
635 of Arabidopsis to High Irradiance. Plant Physiol **144**: 1391–1406
636 **Koroleva OA, Gibson TM, Cramer R, Stain C** (2010) Glucosinolate-accumulating S-cells
637 in Arabidopsis leaves and flower stalks undergo programmed cell death at early stages
638 of differentiation. Plant J **64**: 456–469

639 **Leegood RC** (2008) Roles of the bundle sheath cells in leaves of C3 plants. J Exp Bot **59**:
640 1663–1673
641 **Li W, Zhu Z, Chern M, Yin J, Yang C, Ran L, Cheng M, He M, Wang K, Wang J, et al**
642 (2017) A Natural Allele of a Transcription Factor in Rice Confers Broad-Spectrum Blast
643 Resistance. Cell **170**: 114-126.e15
644 **Li Z, Wakao S, Fischer BB, Niyogi KK** (2009) Sensing and Responding to Excess Light.
645 Annu Rev Plant Biol **60**: 239–260
646 **Miller G, Suzuki N, Ciftci-Yilmaz S, Mittler R** (2010) Reactive oxygen species homeostasis
647 and signalling during drought and salinity stresses. Plant, Cell Environ **33**: 453–467
648 **Mittler R, Vanderauwera S, Suzuki N, Miller G, Tognetti VB, Vandepoele K, Gollery M,**
649 **Shulaev V, Van Breusegem F** (2011) ROS signaling: The new wave? Trends Plant Sci
650 **16**: 300–309
651 **Miyake H, Maeda E** (1976) Development of bundle sheath chloroplasts in rice seedlings.
652 Can J Bot **54**: 556–565
653 **Muller P** (2001) Non-Photochemical Quenching. A Response to Excess Light Energy. Plant
654 Physiol **125**: 1558–1566
655 **Mullineaux PM, Exposito-Rodriguez M, Laissue PP, Smirnoff N** (2018) ROS-dependent
656 signalling pathways in plants and algae exposed to high light: Comparisons with other
657 eukaryotes. Free Radic Biol Med **122**: 52–64
658 **Mullineaux PM, Karpinski S, Baker NR** (2006) Spatial dependence for hydrogen peroxide-
659 directed signaling in light-stressed plants. Plant Physiol **141**: 346–350
660 **Murchie EH, Niyogi KK** (2011) Manipulation of Photoprotection to Improve Plant
661 Photosynthesis. Plant Physiol **155**: 86–92
662 **Nietzel T, Elsässer M, Ruberti C, Steinbeck J, Ugalde JM, Fuchs P, Wagner S,**
663 **Ostermann L, Moseler A, Lemke P, et al** (2019) The fluorescent protein sensor
664 roGFP2-Orp1 monitors in vivo H(2) O(2) and thiol redox integration and elucidates
665 intracellular H(2) O(2) dynamics during elicitor-induced oxidative burst in Arabidopsis.
666 New Phytol **221**: 1649–1664
667 **Noctor G, Foyer CH** (1998) ASCORBATE AND GLUTATHIONE: Keeping Active Oxygen
668 Under Control. Annu Rev Plant Physiol Plant Mol Biol **49**: 249–279
669 **O'Donnell B V, Tew DG, Jones OT, England PJ** (1993) Studies on the inhibitory

670 mechanism of iodonium compounds with special reference to neutrophil NADPH
671 oxidase. Biochem J **290 (Pt 1**: 41–49
672 **Patro R, Duggal G, Love MI, Irizarry RA, Kingsford C** (2017) Salmon provides fast and
673 bias-aware quantification of transcript expression. Nat Methods **14**: 417–419
674 **Rossel JB, Wilson IW, Pogson BJ** (2002) Global Changes in Gene Expression in
675 Response to High. Society **130**: 1109–1120
676 **Ruban A V** (2016) Nonphotochemical Chlorophyll Fluorescence Quenching: Mechanism
677 and Effectiveness in Protecting Plants from Photodamage. Plant Physiol **170**: 1903–
678 1916
679 **Ruckle ME, Burgoon LD, Lawrence LA, Sinkler CA, Larkin RM** (2012) Plastids Are Major
680 Regulators of Light Signaling in Arabidopsis. Plant Physiol **159**: 366–390
681 **Sade N, Shatil-Cohen A, Attia Z, Maurel C, Boursiac Y, Kelly G, Granot D, Yaaran A,**
682 **Lerner S, Moshelion M** (2014) The Role of Plasma Membrane Aquaporins in
683 Regulating the Bundle Sheath-Mesophyll Continuum and Leaf Hydraulics. Plant Physiol
684 **166**: 1609 LP – 1620
685 **Sadey N, Shatil-Cohen A, Moshelion M** (2015) Bundle-sheath aquaporins play a role in
686 controlling Arabidopsis leaf hydraulic conductivity. Plant Signal Behav **10**: 1–4
687 **Sage RF** (2001) Environmental and Evolutionary Preconditionsfor the Origin and
688 Diversification of the C4 PhotosyntheticSyndrome. Plant Biol **3**: 202–213
689 **Schachtman DP, Goodger JQD** (2008) Chemical root to shoot signaling under drought.
690 Trends Plant Sci **13**: 281–287
691 **Shatil-Cohen A, Attia Z, Moshelion M** (2011) Bundle-sheath cell regulation of xylem-
692 mesophyll water transport via aquaporins under drought stress: a target of xylem-borne
693 ABA? Plant J **67**: 72–80
694 **Smirnoff N, Arnaud D** (2019) Hydrogen peroxide metabolism and functions in plants. New
695 Phytol **221**: 1197–1214
696 **Thordal-Christensen H, Zhang Z, Wei Y, Collinge DB** (1997) Subcellular localization of
697 H2O2 in plants. H2O2 accumulation in papillae and hypersensitive response during the
698 barley-powdery mildew interaction. Plant J **11**: 1187–1194
699 **Vogel MO, Moore M, Konig K, Pecher P, Alsharafa K, Lee J, Dietz K-J** (2014) Fast
700 Retrograde Signaling in Response to High Light Involves Metabolite Export, MITOGEN-

701 ACTIVATED PROTEIN KINASE6, and AP2/ERF Transcription Factors in Arabidopsis.
702 Plant Cell **26**: 1151–1165
703 **Wang X, Zhang M-M, Wang Y-J, Gao Y-T, Li R, Wang G-F, Li W-Q, Liu W-T, Chen K-M**
704 (2016) The plasma membrane NADPH oxidase OsRbohA plays a crucial role in
705 developmental regulation and drought-stress response in rice. Physiol Plant **156**: 421–
706 443
707 **Winterbourn CC** (2014) The challenges of using fluorescent probes to detect and quantify
708 specific reactive oxygen species in living cells. Biochim Biophys Acta **1840**: 730–738
709 **Yoshida T, Fernie AR** (2018) Remote Control of Transpiration via ABA. Trends Plant Sci **23**:
710 755–758
711 **Zandalinas SI, Mittler R** (2018) ROS-induced ROS release in plant and animal cells. Free
712 Radic Biol Med **122**: 21–27
713

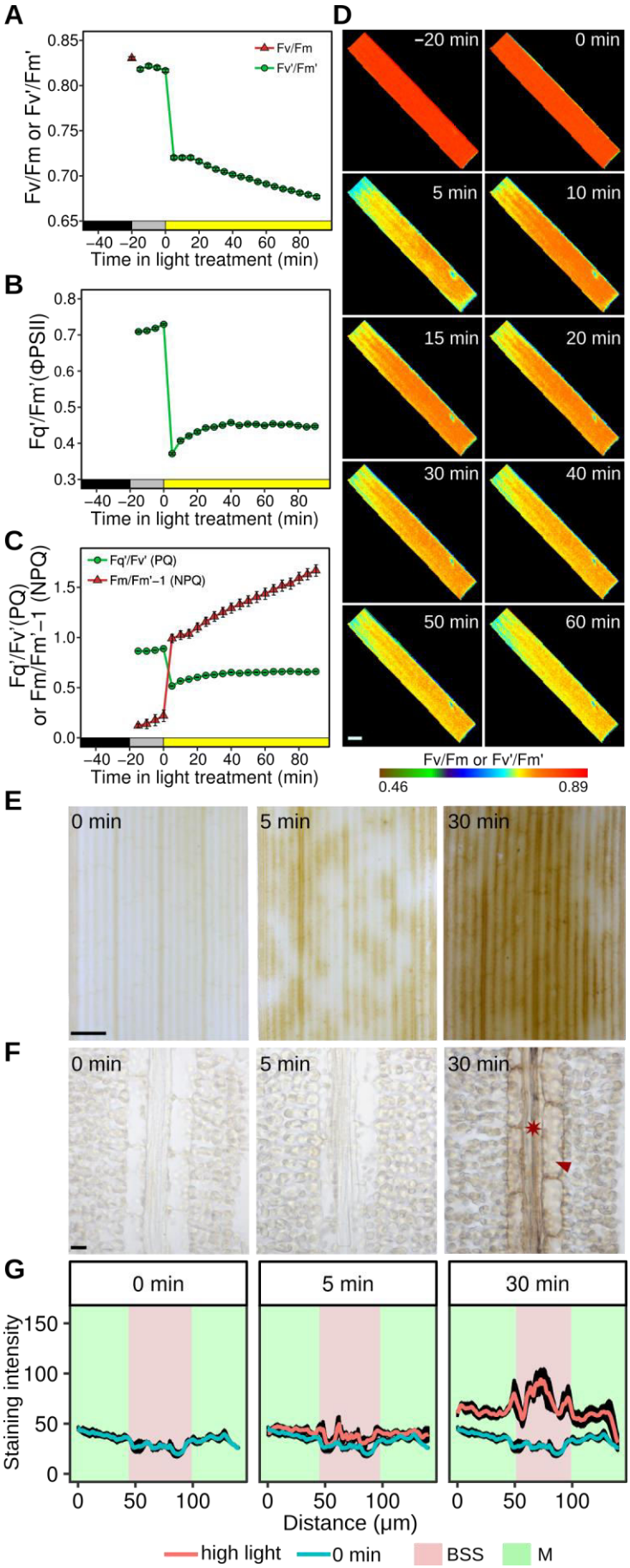

Figure 1. Rice bundle sheath strands preferentially accumulate the DAB polymerization product in response to high light. (A-C) Chlorophyll fluorescence parameters associated with dark-adapted leaves being moved into the light intensity of growth for 20 min, and then moved to a 10-fold higher intensity of light. (A) Dark-adapted F_v/F_m and F_v'/F_m' (B) Quantum efficiency of PSII (F_q'/F_m' or ΦPSII) and (C) Photochemical (PQ) and Non Photochemical Quenching (NPQ). Data shown represent mean and standard error from 16 leaves. (D) Representative images from the chlorophyll fluorescence imager showing responses were reasonably homogenous across the leaf. Scale bar = 2 mm. (E) High light stress led to strong staining from the DAB polymerization product in bundle sheath strands arranged along the proximal to distal axis of the leaf blade. After five minutes of high light staining is evident, but at thirty minutes it is stronger and more homogenous in these bundle sheath strands. Scale bar = 1 mm. (F) Representative image from paradermal sections show that cells accumulating DAB stain are veins (asterisk) and bundle sheath cells (arrowhead). Scale bar = 10 µm. (G) Quantitation of DAB stain in mesophyll and bundle sheath strands. Data are presented as mean (red or blue line) and one standard error from the mean, n= 4).

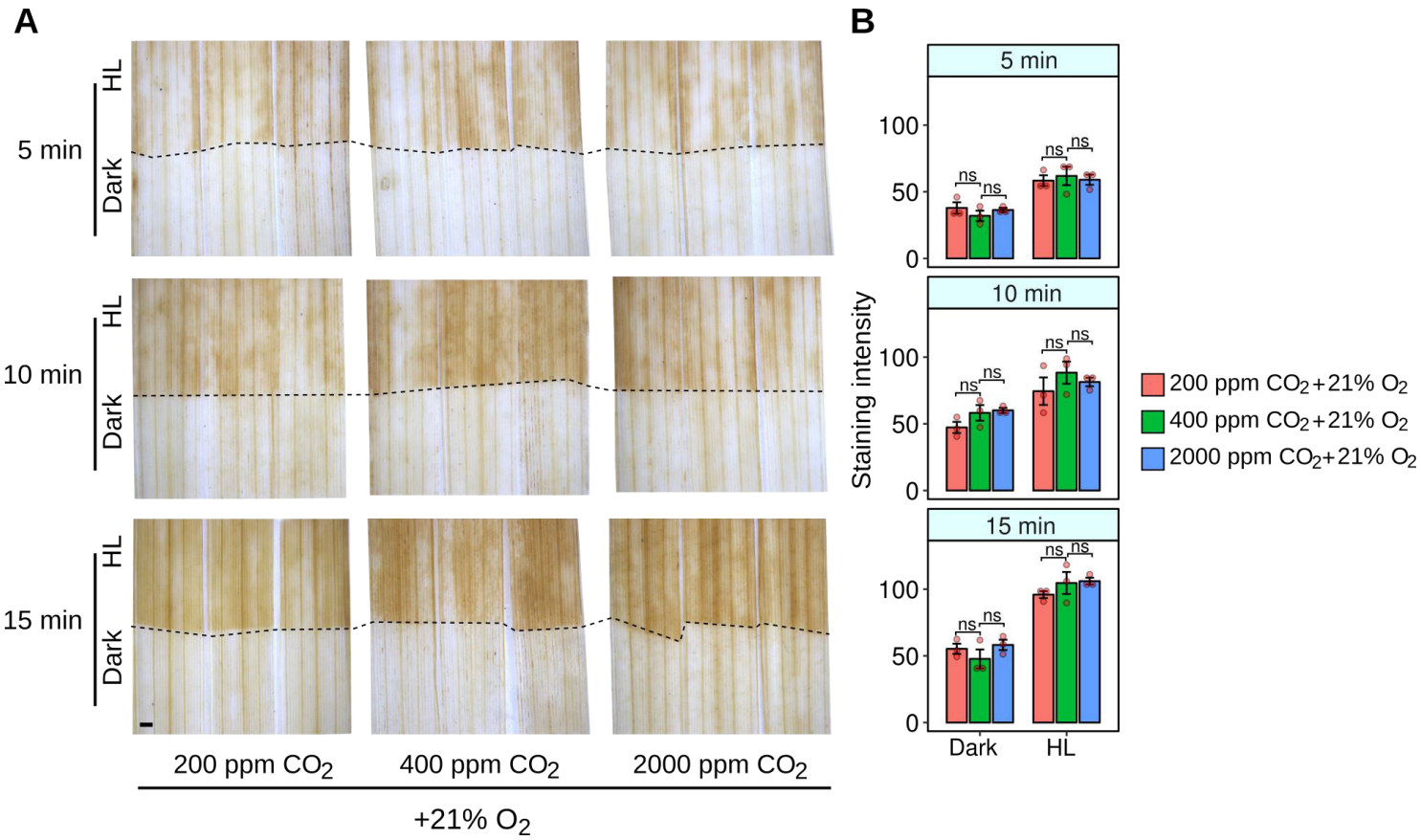

Figure 2. Altering CO_2 supply has little effect on the high light response of the rice bundle sheath. (A) Neither reducing (200 ppm) nor increasing (2000 ppm) CO_2 had a clear effect on DAB staining at 21% oxygen. (B) Quantitation of DAB staining of leaves subjected to low or high CO_2. ANOVA indicated no significant statistical difference associated with CO_2 treatment (p=0.22). Scale bar represents 1 mm.

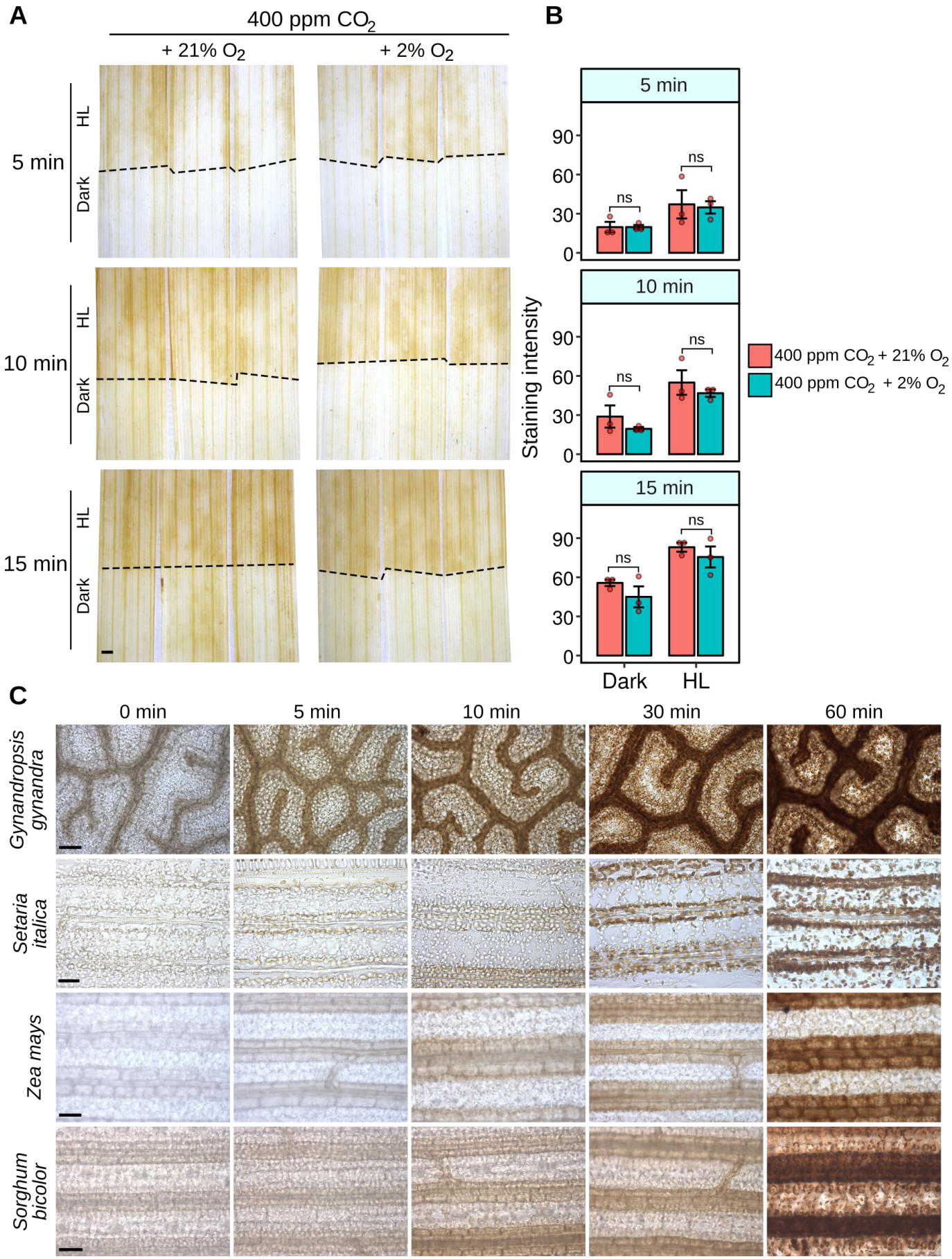

Figure 3. Photorespiration is not the source of the high light dependent accumulation of DAB stain in bundle sheath strands. (A) Representative images of DAB staining leaves exposed to 750 µmol m^{-2} sec^{-1} photon flux density for 5, 10 or 15 mins in 400 ppm CO_2 and either 21% or 2% O_2. Photorespiration is limited by 2% O_2. (B) Quantification of DAB staining. ANOVA indicated no significant statistical difference associated with O_2 treatment (p=0.0933). (C) DAB staining leaves of C_4 plants *Gynandropsis gynandra*, *Setaria italica, Zea mays, Sorghum bicolor* exposed to high light. Although C_4 plants have limited photorespiration in the bundle sheath, DAB staining was still detected in this tissue. Scale bars represent 1 mm (A) and 50 µm (B).

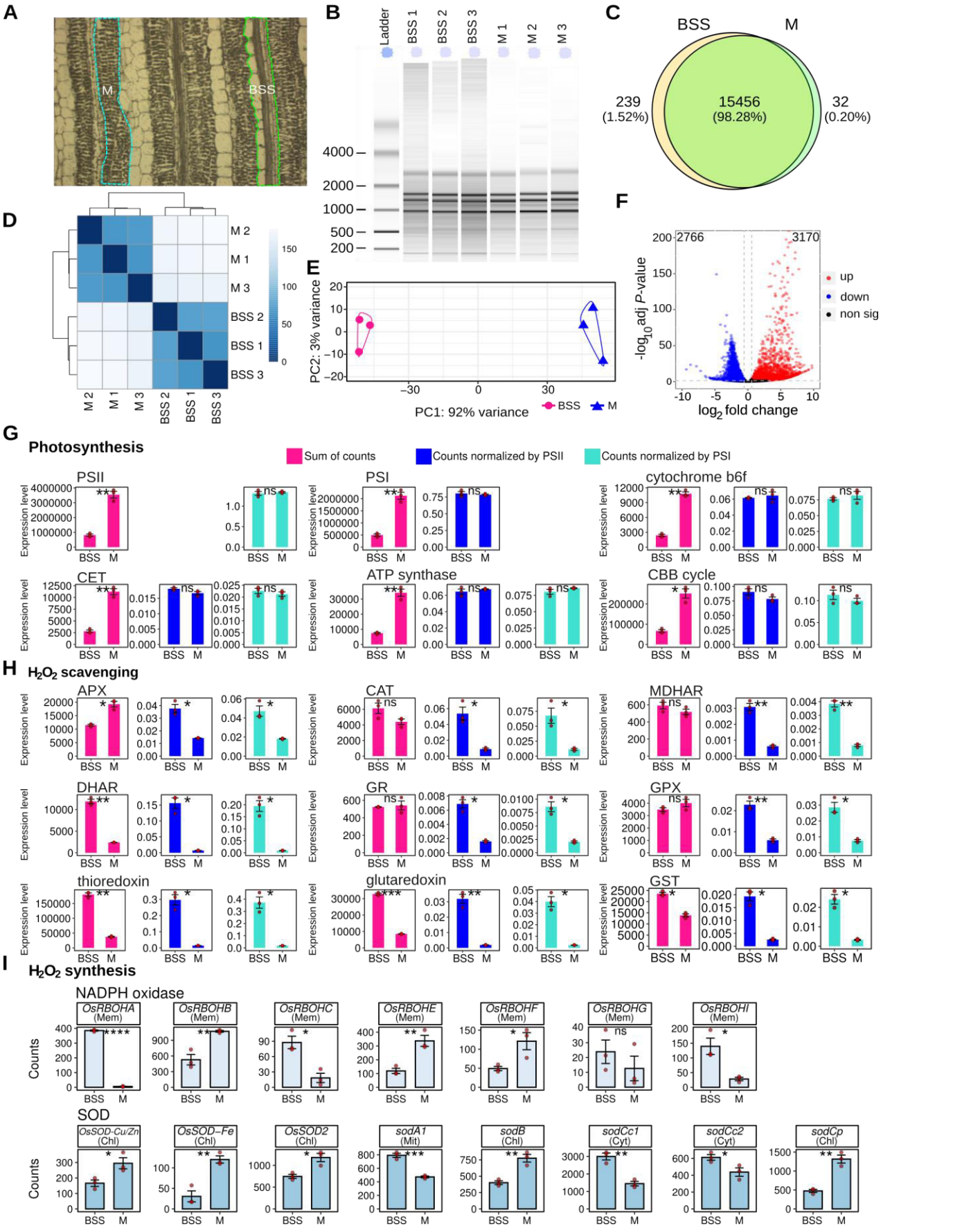

Figure 4. Global analysis mRNA from bundle sheath strands (BSS) and mesophyll (M) cells indicates balanced accumulation of transcripts encoding components of the photosynthetic electron transport chain and the Calvin Benson cycle, but that bundle sheath strands may have greater capacity to synthesise reactive oxygen species. (A) Bundle sheath strands (BSS) and mesophyll (M) were sampled for RNA using laser capture microdissection. (B) Electropherogram showing RNA quality. (C) Pie chart summarizing number of genes expressed in both BSS and M cells. (D) Hierarchical dendrogram and (E) Principal Component Analysis indicate that most variance was associated with tissue type. (F) Volcano plot showing number of differentially expressed genes between BSS and M. (G-I) Abundance of photosynthesis (G), H_2O_2 scavenging (H) and H_2O_2 synthesis (I) transcripts. For photosynthesis complexes the sum of all components of each complex is presented, and to take into account lower chloroplast content in bundle sheath strands these were normalized to either Photosystem I or II. Predicted subcellular localization of each NADPH oxidase (RBOH) and Superoxide dismutase (SOD) isoform is annotated (chl = chloroplast, mem = plasma membrane, mit = mitochondrial, cyt = cytoplasm.). T-tests indicate statistically significant differences (**** $p < 0.0001$, *** $p < 0.001$, ** $p < 0.01$, * $p < 0.05$).

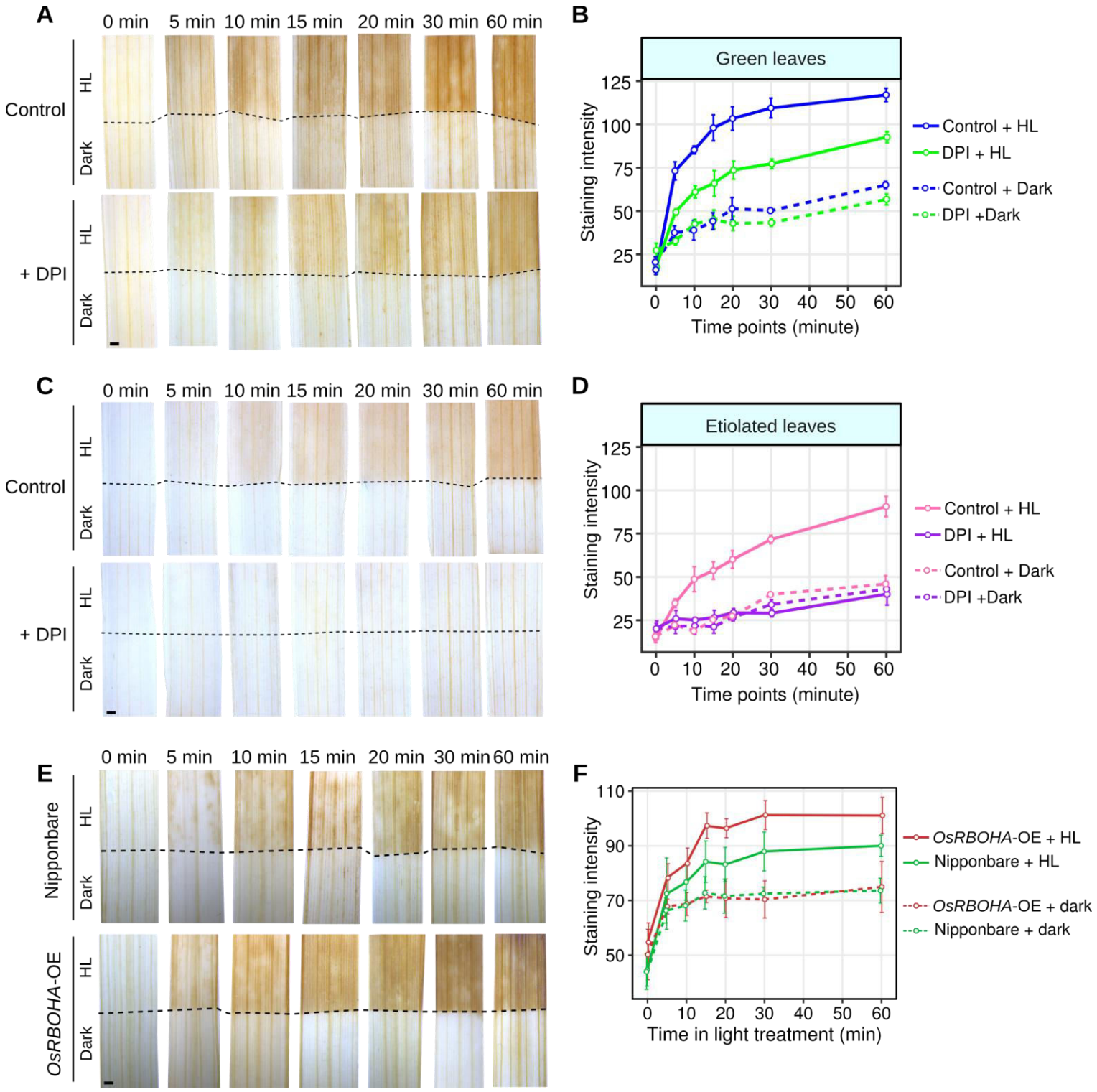

Figure 5. Inhibiting and increasing NADPH oxidase reduces and increases DAB staining respectively in bundle sheath strands of rice leaves. (A) Diphenyleneiodonium (DPI) a plasma membrane NAD(P)H oxidase inhibitor, partially inhibits DAB staining in bundle sheath strands of green leaves. (B) Quantitation of DAB staining over time in control compared with DPI and high light treated green leaves. (C) DPI completely inhibits DAB staining in etiolated leaves. (D) Quantitation of DAB staining over time in control and DPI high light treated etiolated leaves. (E) Overexpression of *OsRBOHA* increased DAB staining in bundle sheath strands after high light treatment. (F) Quantitation of DAB staining over time in green leaves from either the control or *OsRBOHA* overexpression line. In all cases the lower portion of the leaf (below the dotted line) was covered to provide an in-leaf control over the time-course. ANOVA showed DAB staining was reduced after DPI treatment in green leaves ($p<0.001$), etiolated leaves ($p<0.001$), and increased in *RBOHA* over-expressors ($p<0.05$). Scale bars represent 1 mm.

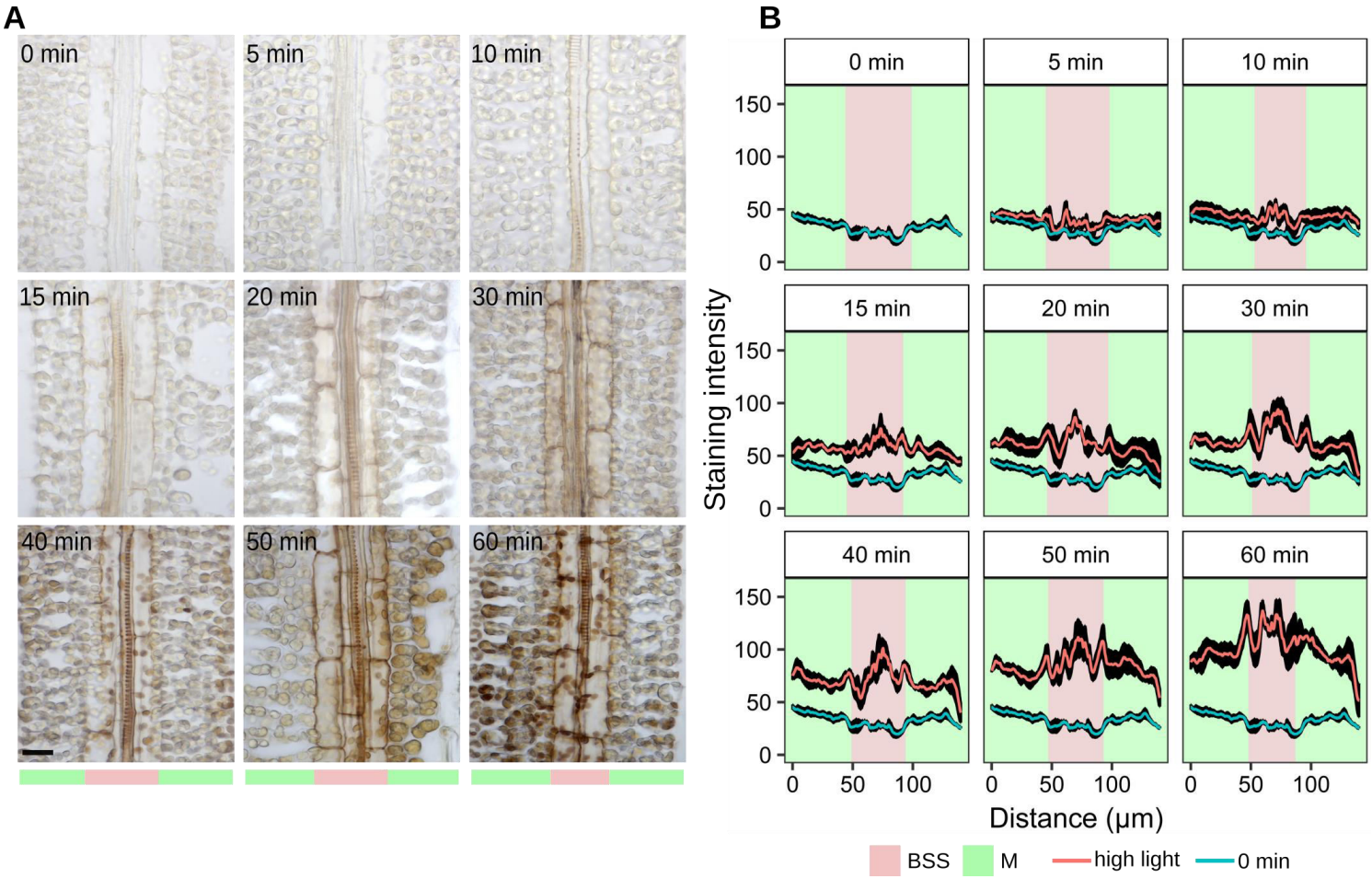

Figure S1. DAB staining of paradermal sections from rice leaves exposed to high light. (A) Representative images of leaves exposed to 750 µmol m^{-2} s^{-1} photon flux density for 0, 5, 10, 15, 20, 30, 40, 50 or 60 minutes. Brown stain indicates the formation of the polymerization product formed in the presence of reactive oxygen species. Scale bar denotes 10 µm. (B) Quantitation (arbitrary units) of DAB staining from paradermal sections illustrating the extent to which reactive oxygen species are first detected in vein and bundle sheath strands versus mesophyll cells The x-axis represents a scan from left to right across the paradermal sections. The y-axis depicts gray values extracted from paradermal sections. Data are presented as mean (red or blue line) and one standard error from the mean, n = 4). The response of bundle sheath strands to high light was greater than that of mesophyll cells (Two-way ANOVA $p < 0.001$).

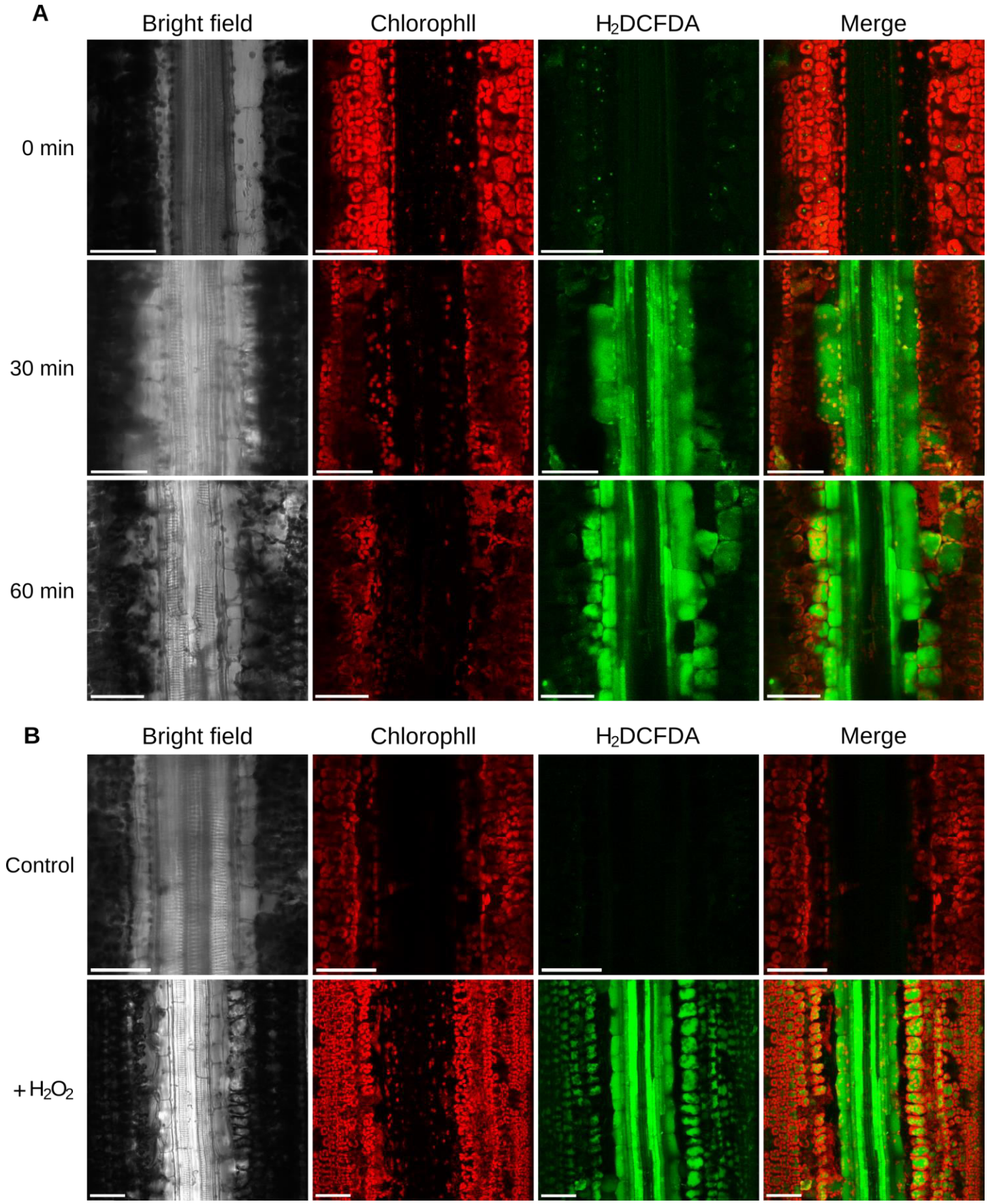

Figure S2. Confocal scanning microscopy indicates bundle sheath preferential fluorescence from H_2DCFDA in rice leaves exposed to high light. (A) Representative images of leaves were fed with 10 µM H_2DCFDA for 12 h prior to being exposed to high light (750 µmol m^{-2} s^{-1} photon flux density) for the times indicated. (B) Representative images from control leaves suppled with water as well as those suppled with 10 µM H_2DCFDA and exogenous 100 mM H_2O_2. Fluorescence from H_2DCFDA was not detected in control leaves, but in those to which H_2O_2 had been added it was detected in both mesophyll and bundle sheath strands. Scale bars denote 50 µm.

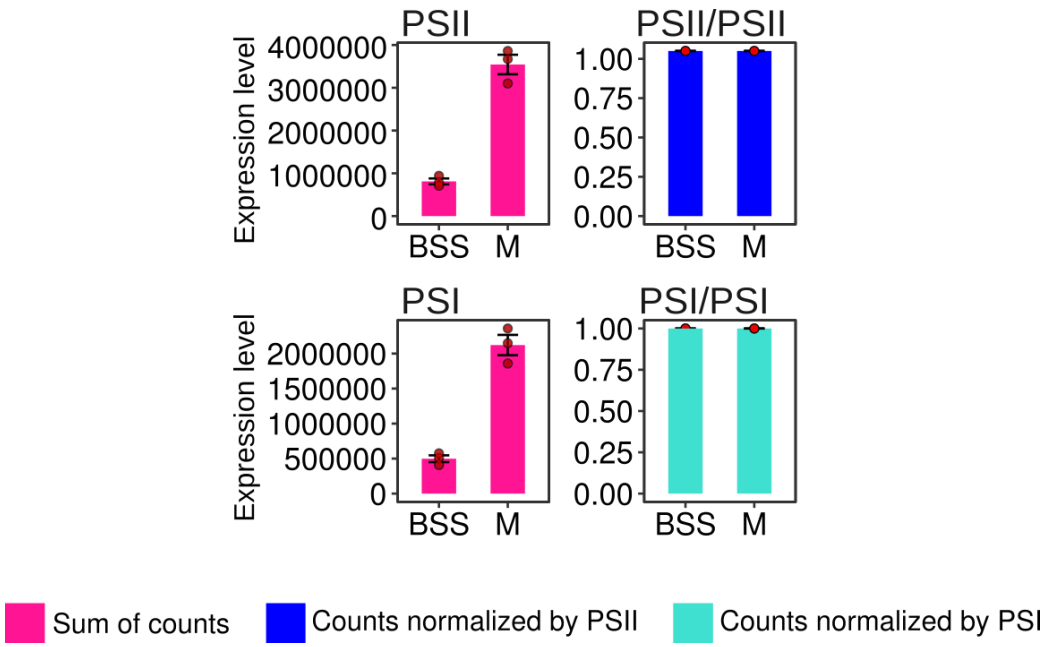

Figure S3. Normalisation of PSII and PSI against themselves indicates the expected one-to-one relationship.

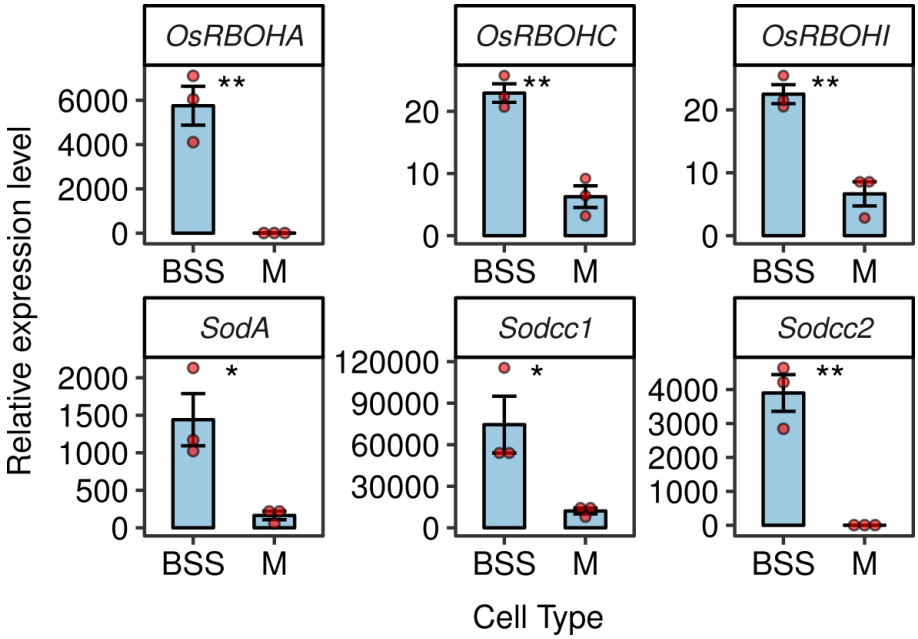

Figure S4. qPCR confirms analysis from deep sequencing and shows that transcripts of *RBOHA, RBOHC & RBOHI* as well as *SODA, SODCC1 & SODCC2* are more abundant in bundle sheath stands (BSS) than mesophyll (M) cells. RNA extracted from green leaves. Data are normalized to *OsUBQ5* as a control and presented as mean ± one standard error, n = 3. T-tests indicate statistically significant differences (** $p < 0.01$, * $p < 0.05$).

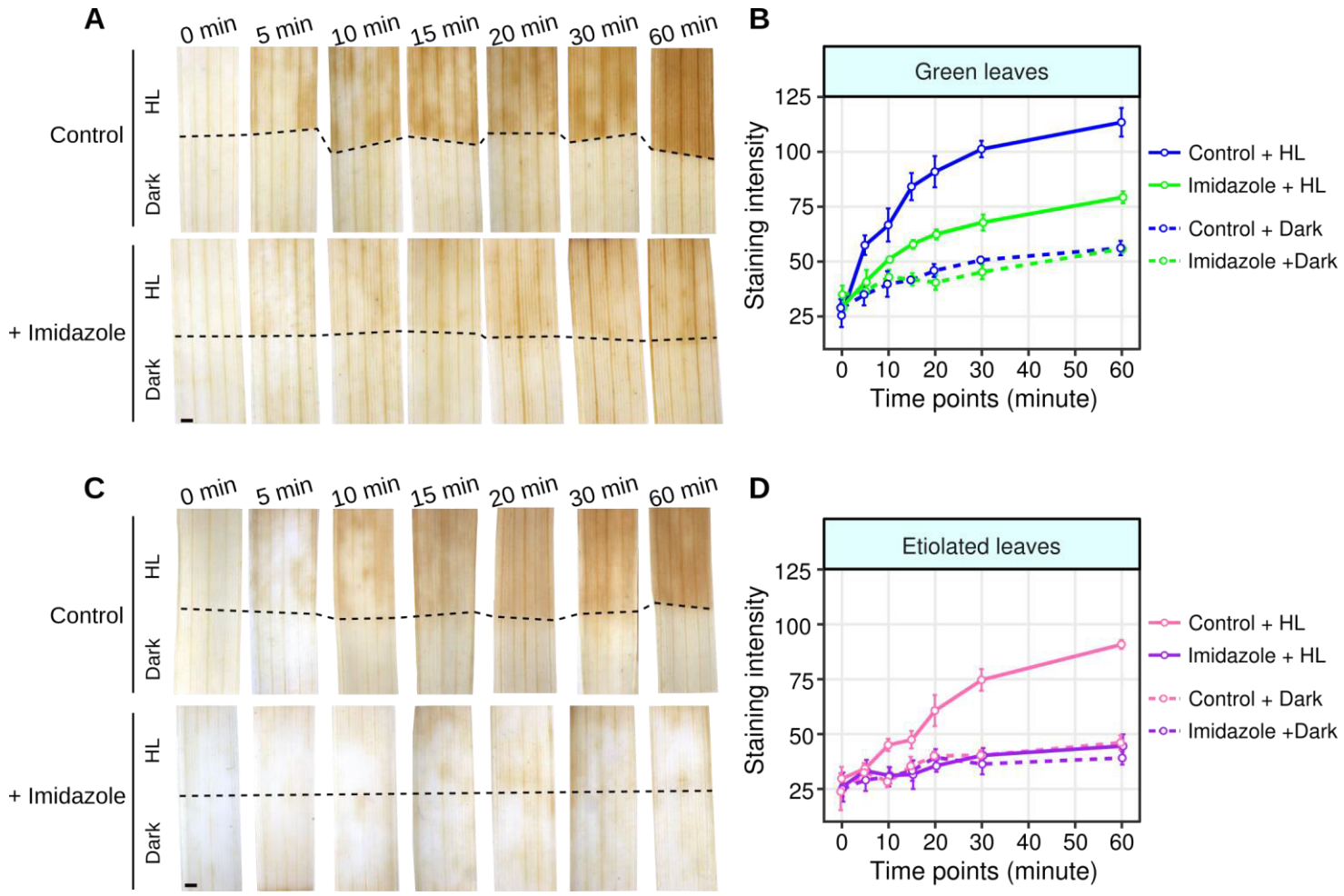

Figure S5. Inhibiting NAD(P)H oxidase activity with imidazole phenocopies the effect from diphenyleneiodonium in green and etiolated leaves. (A&B) Imidazole partially inhibits the accumulation of DAB in green leaves. (C&D) Imidazole completely inhibits DAB accumulation in etiolated leaves. ANOVA showed DAB staining was reduced after Imidazole treatment in green leaves ($p<0.001$), etiolated leaves ($p<0.001$).

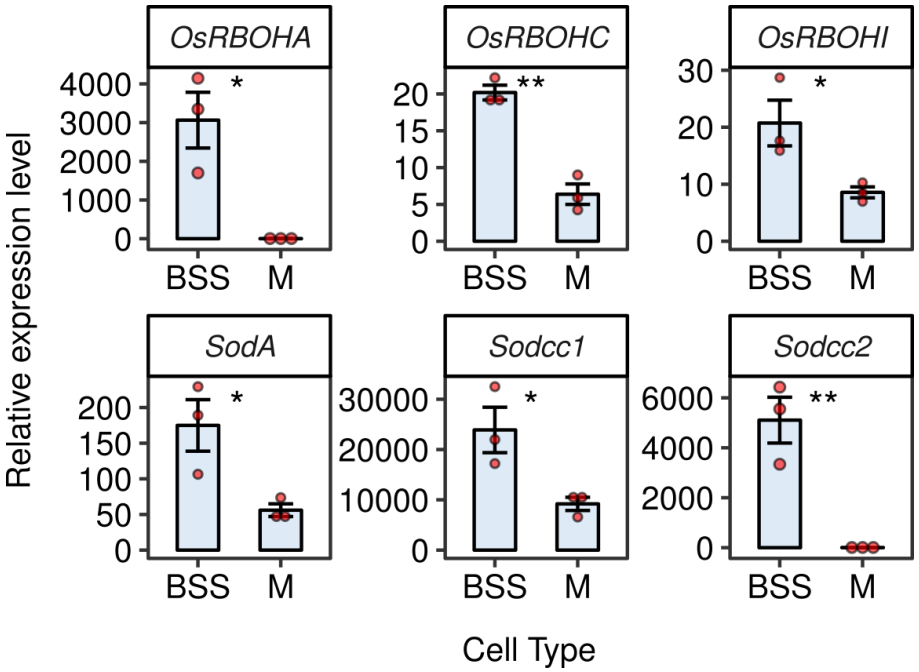

Figure S6. Q-PCR shows that transcripts encoding *OsRBOHA, RBOHC & RBPOHI* as well as *SODA, SODCC1 &SODCC2* are more abundant in bundle sheath strands than mesophyll ells in etiolated leaves of rice. *OsUBQ5* was used to normalize expression of each gene, and data are presented as the mean ± one standard error, n = 3. T-tests showed statistically significant difference between bundle sheath strands (BSS) and mesophyll (M) cells with ** = p< 0.01, * = p < 0.05.

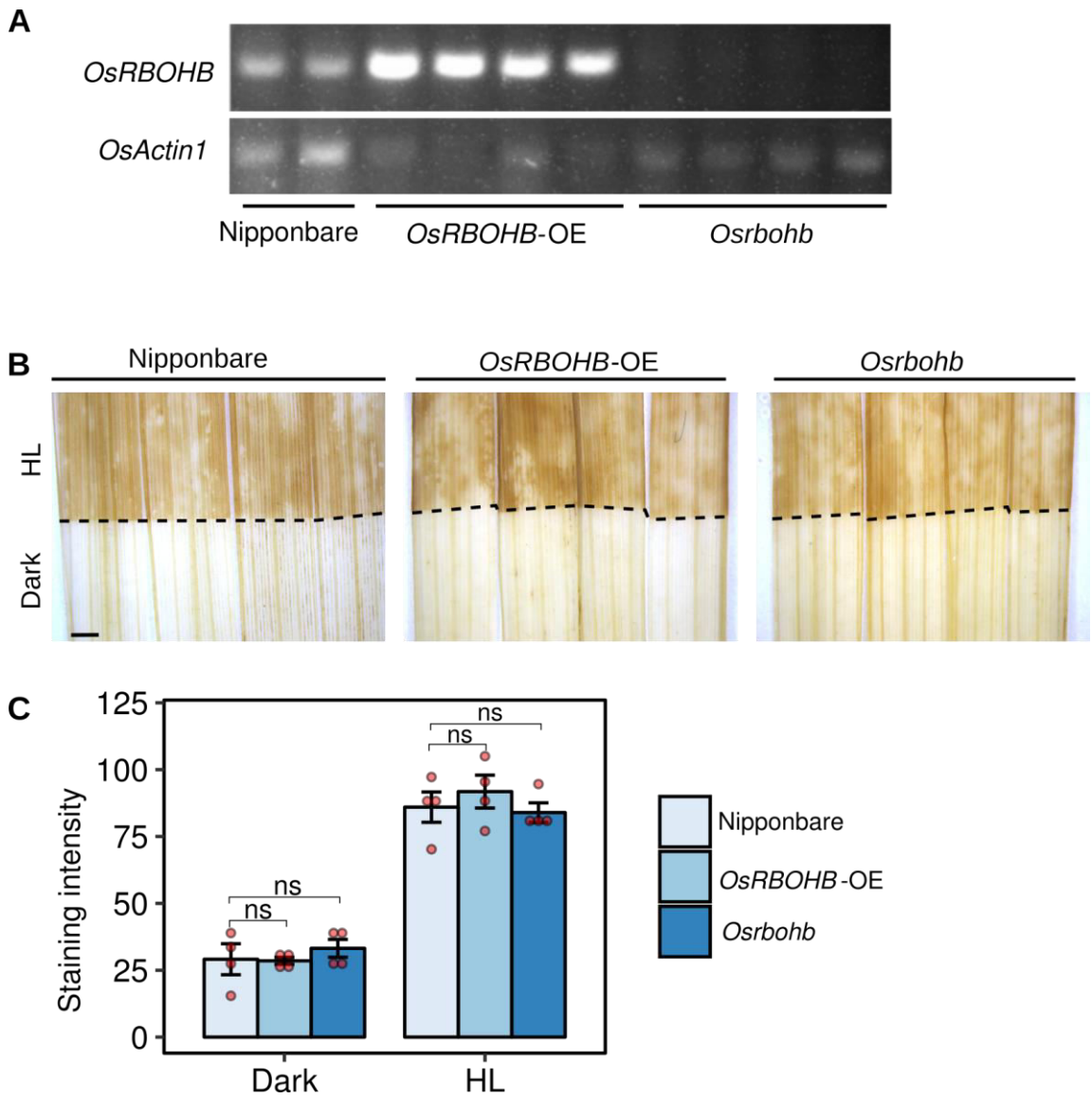

Figure S7. The *RBOHB* gene appears not to be involved in the high light response of the rice bundle sheath. (A) Semi-quantitative RT-PCR indicating that compared with the Nipponbare control, an over-expression line (*OsRBOHB-OE*) and a mutant allele (*Osrbohb*) contain increased and reduced transcripts from *RBOHB* respectively. *ACTIN1* is shown below as a control. (B) Representative images showing that the over-expression line and mutant allele of *RBOHB* show no difference in DAB staining compared with the Nipponbare control. (C) Quantification of DAB staining in (B). Scale bar represents 2 mm. T-tests showed that there was no significant (ns) statistical differences associated with over-expression of *OsRBOHB*.

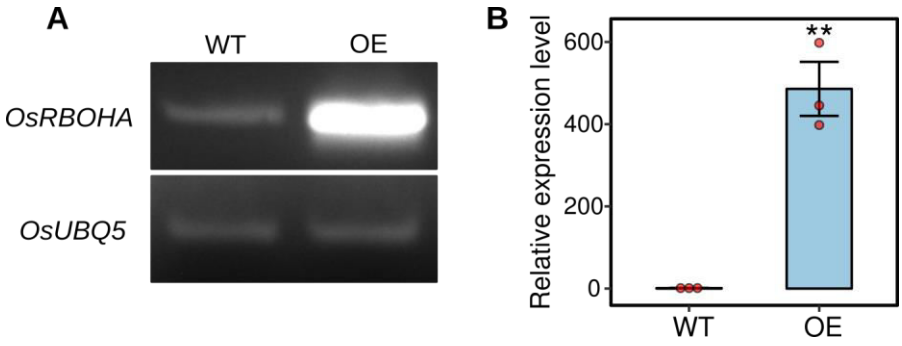

Figure S8. RT-PCR (A) and Q-PCR (B) were used to confirm over-expression of *OsRBOHA* compared with wild type (WT). *OsUBQ5* was used as a control. T-test showed statistically significant difference in the over-expressor (OE) compared with wild type (WT) ($p<0.01$).

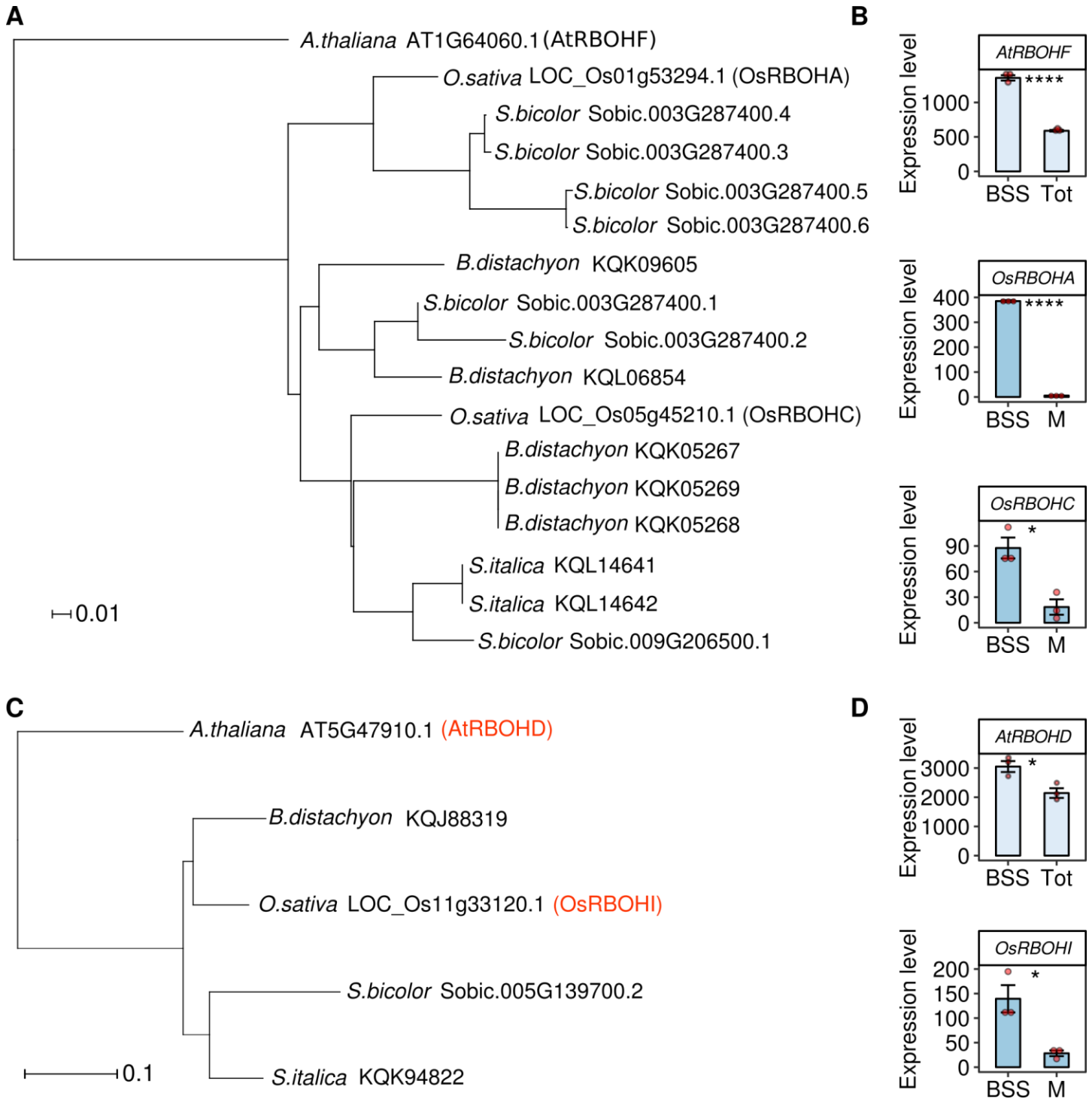

Figure S9. Phylogenetic reconstructions of *RBOH* genes depicting orthology relationships between those from rice, *Arabidopsis thaliana, Sorghum bicolor,* and *Brachypodium distachyon*. (A) Phylogenetic reconstruction indicating likely relationship between *AtRBOHF* and related genes in the grasses. (B) Transcript abundance of *AtRBOHF* in bundle sheath strands and total leaf material of *A. thaliana,* and of *OsRBOHA* and *OsRBOHC* in bundle sheath strands and mesophyll cells of rice. (C) Phylogenetic reconstruction indicating likely relationship between *AtRBOHD* and related genes in the grasses. *AtRBOHD* and *OsRBOHI* are highlighted in red. (D) Transcript abundance of *AtRBOHD* in bundle sheath strands and total leaf material or *A. thaliana* and of *OsRBOHI* in bundle sheath strands and mesophyll cells of rice. T-tests show statistically significant differences between cell type **** = $p < 0.0001$, * = $p < 0.05$.